The Thesis Committee for Peter John Schemper
Certifies that this is the approved version of the following Thesis:

Depositional Systems, Lithofacies, and Geochemistry of the Jurassic (Oxfordian) Smackover and Buckner Formations in Van Zandt County, Texas: A Type-Core Section

APPROVED BY
SUPERVISING COMMITTEE:

Supervisor: _____
Robert G. Loucks

Co-Supervisor: _____
Qilong Fu

_____
Charles Kerans

_____
Laura Zahm

Depositional Systems, Lithofacies, and Geochemistry of the Jurassic (Oxfordian) Smackover and Buckner Formations in Van Zandt County, Texas: A Type-Core Section

by

Peter John Schemper

Thesis

Presented to the Faculty of the Graduate School of

The University of Texas at Austin

in Partial Fulfillment

of the Requirements

for the Degree of

Master of Science in Geological Science

The University of Texas at Austin

May, 2019

Dedication

To my parents, Tom and Susan Schemper, and my brothers, Jake and Ben Schemper, for supporting me and motivating me.

Acknowledgements

I would like to express my gratitude to those who accepted me into the University of Texas at Austin graduate program, Qilong Fu and Robert G. Loucks. If it weren't for their interest in me as a student, I would not have had this amazing opportunity. I am grateful for the mentorship and guidance of Robert G. Loucks. I would also like to thank Charles Kerans and Laura Zahm for being on my committee and teaching me through the master's program.

I would like to thank Equinor for granting me a fellowship and funding my research. Additionally, I would like to thank STARR for funding me prior to receiving a fellowship and Mudrock Systems Research Laboratory (MSRL) and Reservoir Characterization Research Laboratory (RCRL) for welcoming me as a participant in their consortium meetings.

I would like to thank the staff at the Bureau of Economic Geology core research center for allowing me to keep my core displayed for a substantial amount of time, to Evan Sivil, Greg Stefans, and Toti Larson for helping me acquire my XRF and Isotope datasets, and to Tobi Kosaki, James Green, and Paul Linton at ALS Oil and Gas for collaborating and scanning the core for hyperspectral analysis.

Finally, I would like to thank my parents for nurturing me into the person I am today and providing me the opportunities that led me here. I would also like to thank my brothers for showing me how to be a better person and for pushing me to be that person.

Abstract

Depositional Systems, Lithofacies, and Geochemistry of the Jurassic (Oxfordian) Smackover and Buckner Formations in Van Zandt County, Texas: A Type-Core Section

Peter John Schemper, M.S. Geo. Sci.
The University of Texas at Austin, 2019

Supervisors: Robert G. Loucks, Qilong Fu

The Late Jurassic Smackover Formation is part of a prolific petroleum system along the northern rim of the Gulf of Mexico with a long history of exploration. Most investigations into the Smackover have taken place in sub basins east of the East Texas basin and primarily focus on upper Smackover oolitic grainstone reservoirs, but only a few studies have been completed on the lower Smackover source rocks. Because of this, there is a lack of understanding related to the conditions under which the lower Smackover was deposited. This study provides a more complete understanding of the Smackover deposits in the East Texas through investigation of a long continuous 713-ft core drilled from the Sun Oil Travis GU No. 1 well in Van Zandt County, Texas. It contains a continuous section of Smackover lithofacies from lower Smackover mudstones

to upper Smackover grainstones and contains a large portion of the overlying Buckner Anhydrite. The goal of this investigation is to lithologically and chemically characterize the Smackover Formation in order to create a type section for future studies and create a refined depositional model for East Texas Smackover deposition. High-resolution geochemical data composed of x-ray diffraction analysis (XRD), total organic carbon (TOC) and Rock-Eval, x-ray fluorescence (XRF) analysis, and isotope data was taken to fully characterize the section chemically. This geochemical dataset provides insight into controls on organic matter accumulation and destruction, diagenetic fluids, and local and global isotope signatures. With understandings of lithofacies distribution, depositional controls for organic accumulation and porosity development, and diagenesis the unconventional and conventional potential of the Smackover can be assessed.

Table of Contents

List of Figures

CHAPTER 1: INTRODUCTION

The Smackover Formation is a significant hydrocarbon-producing formation along the onshore northern rim of the Gulf of Mexico (GOM) (Locklin, 1984; Mancini, 2003; Pearson, 2011). Production within the Smackover is generally from dolomitized oolitic grainstones and other associated lithofacies in the upper Smackover (Ewing, 2001; Mancini et al, 2003; Pearson, 2011) with the Buckner being the top seal. upper Smackover reservoirs are sourced from organic-rich lower Smackover mudrocks (commonly referred to as the *varved section* or the *Brown Dense*) (Claypool and Mancini, 1989; Sassen, 1990). The Brown Dense is an unconventional reservoir in other areas of the GOM (Walkinshaw, 2017). In the past, it has been questioned whether these organic-rich, laminated mudrocks in the lower Smackover were deposited on a deeper-water ramp (Dickinson, 1968; Budd and Loucks, 1981; Stewart, 1984; Heydari and Baria, 2005) or in a shallow-marine lagoonal environment (inner ramp) (Malek-Aslani, 1973; Mitchell-Tapping, 1984; Hancharik, 1984). These contrasting interpretations pose a significant problem because they undermine the understanding of depositional processes, shoreline locations, relative sea-level oscillations for the given time period, and origin of potential source rock. Without a clear understanding of the depositional environments and sequence stratigraphy of the lower Smackover, it is difficult to assess the origin, potential, and regional distribution of this potential unconventional reservoir.

In this study, a continuous long (713 ft) core from Van Zandt county, Texas—the Sun Oil Travis GU No. 1—was available to characterize the nearly complete section of

the Smackover and much of the Buckner anhydrite section. This well had an initial production of 13,639 million cubic ft per day (Mcf/d) of natural gas. The core contains 95% (592 ft) of the Smackover Formation and 60% of the overlying Buckner anhydrite (121 ft). It covers the complete spectrum of Smackover facies, ranging from organic-rich laminated mudstones to skeletal and oolitic grainstones. Geochemical and lithologic analyses are integrated to develop a high-resolution stratigraphic section that can aid in characterizing the depositional systems, reservoir characteristics, and sealing capabilities of the Smackover and Buckner sections. The objectives of this study are: (1) Develop a refined depositional model for the Smackover and Buckner units in northeastern Texas, (2) Integrate lithologic descriptions and geochemical datasets to provide insight on depositional setting and palaeoceanographic conditions during Smackover and Buckner times, (3) Evaluate unconventional and conventional reservoir quality for the Smackover Formation, and (4) Create a type section for use in defining Smackover and Buckner lithofacies and associated reservoir characteristics in East Texas.

An improved understanding of the Smackover—Buckner petroleum system will contribute to the continued exploration of age-equivalent conventional and unconventional targets and associated source-rocks of Smackover plays along onshore and possibly offshore GOM including the Mexican eastern continental margin.

CHAPTER 2: REGIONAL GEOLOGY AND DEPOSITIONAL HISTORY OF THE EAST TEXAS AREA

The dominant structural features controlling the deposition of late Jurassic sediments formed during rifting events in the late Triassic to Middle Jurassic which resulted in the formation of the Gulf of Mexico (Fig. 1) (Pilger, 1981; Jackson, 1982; Ewing, 2001; Pindell and Kennen, 2001). A series of failed rift zones landward of the main rifting event led to the formation of salt basins along the modern-day northern GOM (Jackson and Seni, 1983). The basins are separated by elevated basement features that are interpreted as areas of little or no rifting or extension of the lithosphere (Ewing, 2009) (Fig. 1). Following Jurassic rifting the basins experienced separate subsidence histories (Ewing, 2009). Linear elevated features such as the Angelina Caldwell Flexure and the Wiggins Arch separate the interior basins from the Gulf of Mexico and may have restricted the basins from receiving influx of sea-water (Fig. 1) (Wood and Walper, 1974).

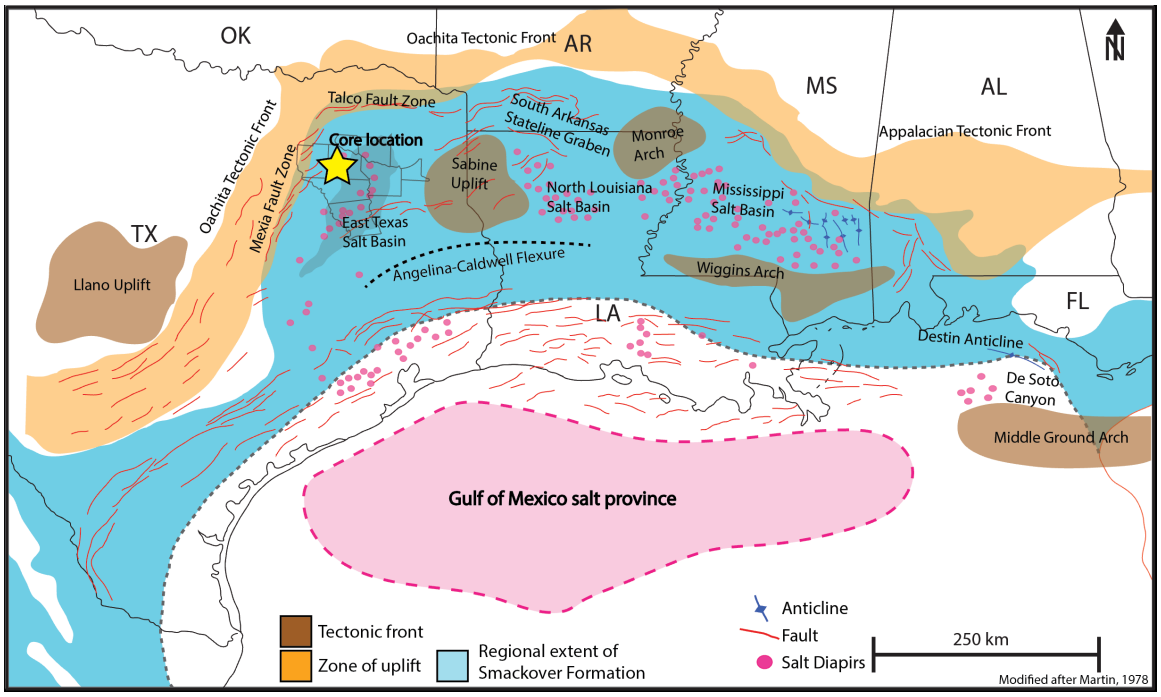

Figure 1: Map of the major structural features along the northern Gulf of Mexico. The location of the Travis Gas Unit No. 1 well is highlighted with a gold star. Figure is modified from Martin (1978).

The East Texas basin is bounded on its east by the Sabine Uplift and to its west and north by the Mexia and Talco fault zones (Fig. 2) (Jackson, 1982). The fault zones are aligned with the up-dip edge of the Louann Salt and formed as gravity slippage of overburden basinward on the Louann Salt which acted as a weak decollement surface (Jackson, 1982). Migration of basinal salts are interpreted as occurring towards the end of Smackover deposition as Jurassic sediments began to prograde into the basin. Mobilization of the salt created complex structural features and faulting that impacted sedimentation throughout the East Texas basin. (Jackson, 1982). Faulting in the Mexia-Talco fault zone and basinal salt structures developed from the late Jurassic to Early Cretaceous and formed migration pathways for hydrocarbons (Jackson and Seni, 1983).

The earliest sediments within the East Texas basin were Triassic and Lower Jurassic red beds of the Eagle Mills Formation (Heydari and Baria, 2005) (Fig. 3). In the late middle Jurassic (Bathonian-Callovian) a transgression led to the formation of restricted hyper saline conditions, depositing the massive Louann Salt and its up-dip equivalent, the Werner Formation (Salvador, 1987; Harwood and Fontana, 1983). Following deposition of the Louann and Werner formations there was a regional sea-level lowstand that led to the deposition of the Norphlet formation (Wade and Moore, 1993). In East Texas, the Norphlet formation was deposited by aeolian or wadi depositional processes.

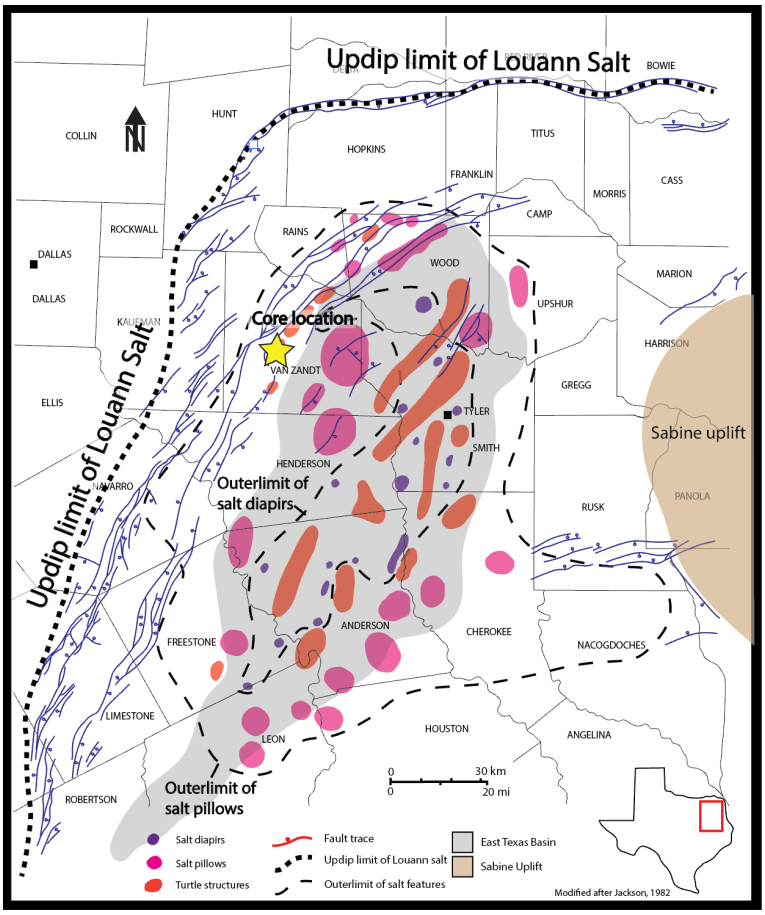

Figure 2: Structural features map of the East Texas Basin. The location of the Travis gas unit No. 1 well is highlighted with a gold star. Figure is modified after Jackson (1982).

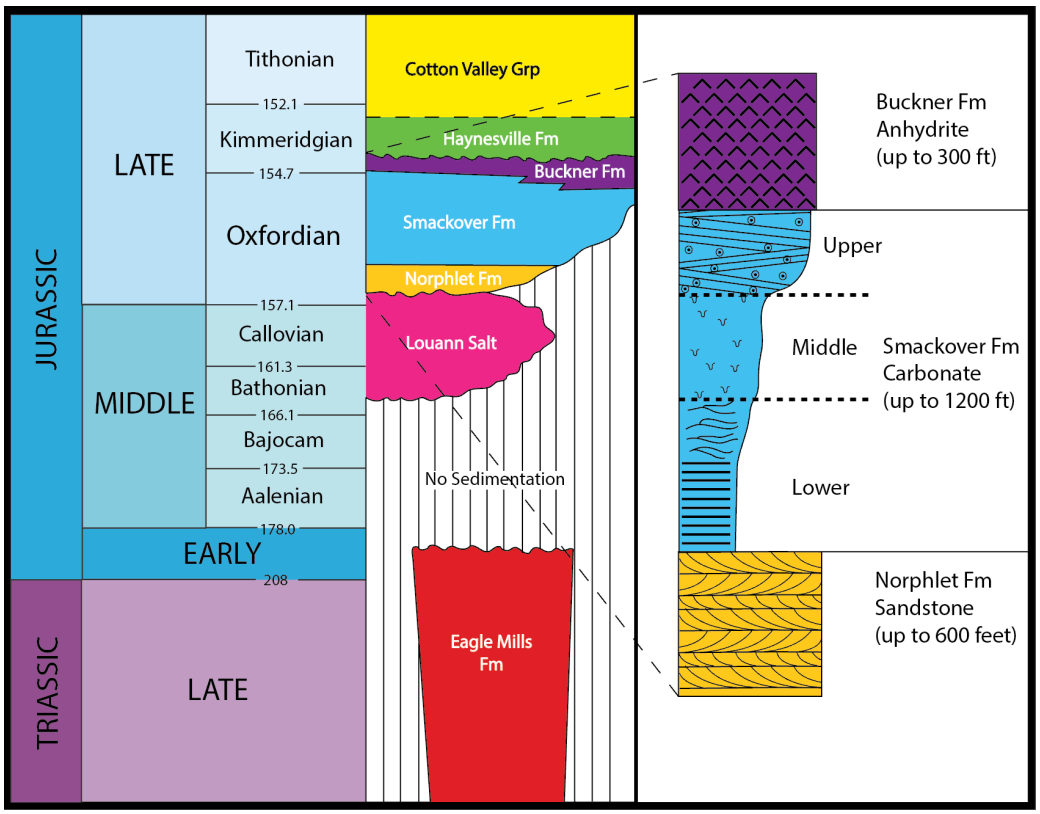

Figure 3: Generalized stratigraphy of the East Texas Basin from late Triassic to late Jurassic. Figure is modified from Heydari and Baria (2006).

Following Norphlet deposition, a second-order transgressive event led to the deposition of the Smackover Formation (Goldhammer, 1998). The sharp contact between the Norphlet Formation and the overlaying Smackover Formation has been interpreted as a transgressive surface, indicating a rapid rise in sea level (Budd and Loucks, 1981). The Smackover has been informally divided into lower, middle, and upper members (Fig. 3) (Dickinson 1968, 1969). The lower member of the Smackover has been described as a finely laminated carbonate mudstone with alternating organic-rich siltstone laminae (Budd and Loucks, 1981; Heydari et al., 1997). This lower section has been informally termed the "varved section" or the "brown dense." The lower section has been interpreted as being deposited in an outer ramp to basinal setting (Budd and Loucks, 1981; Stewart, 1984; Heydari et al., 1997). The middle Smackover is made up of brown carbonate mudstone with varying quantities of peloids, intraclasts, oncoids, and skeletal grains as well as containing burrows and was deposited in a middle ramp setting (Budd and Loucks, 1981; Stewart, 1984; Heydari et al., 1997). The upper section consists of grainstones deposited in high-energy shoals on the inner ramp (Fig. 4) (Budd and Loucks, 1981; Stewart, 1984; Mitchell-Tapping,1984). The Smackover formation forms a wedge that gradually thickens down-dip from approximately 300-400 ft thick to over 1300 ft thick into the basin center of the East Texas basin (Hancharik, 1984).

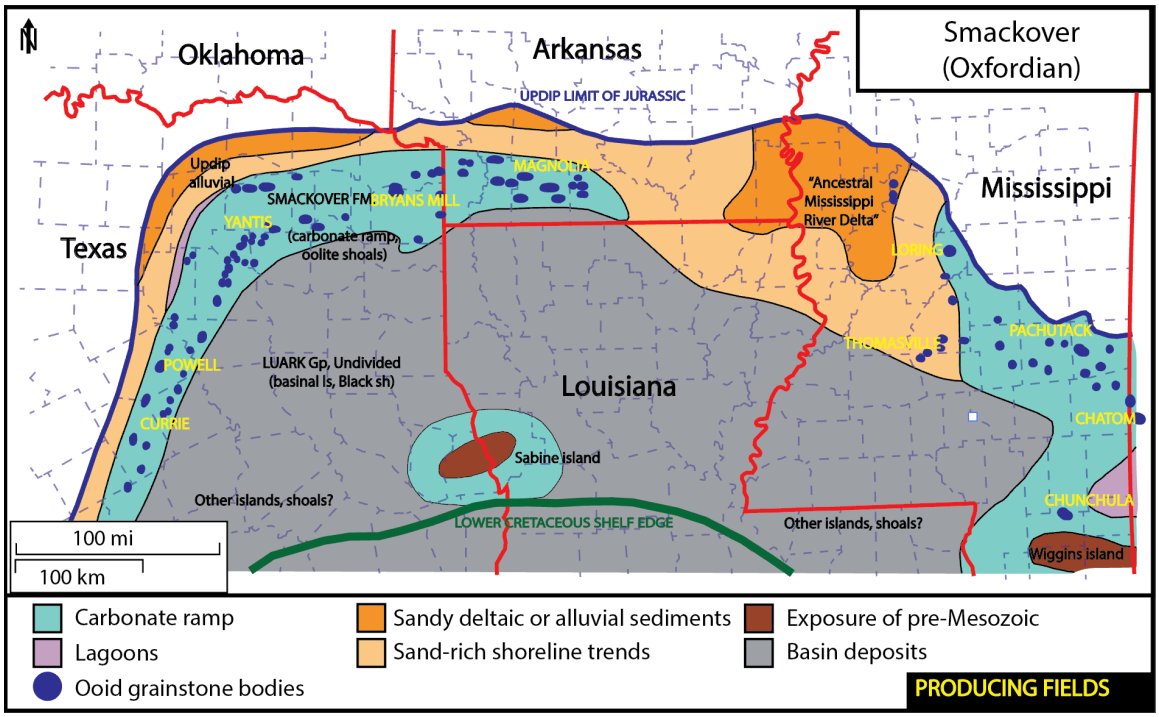

Figure 4: Map of depositional systems of the upper Smackover along the northern Gulf of Mexico during Oxfordian time period. Modified after Ewing, 2001.

In most parts of the East Texas basin the Smackover is overlain by the Buckner Anhydrite, the up-dip portion of the Haynesville Group (Stewart, 1984). The Haynesville Group is composed of the Buckner Anhydrite, upper Buckner, Gilmer limestones and Gilmer shale (Stewart, 1984). There is debate within the literature regarding the contact between the Smackover Formation and the overlying Buckner Anhydrite. Some authors interpreted it as conformable (Mitchell-Tapping, 1984; Hancharik, 1984; Mann, 1988) and others suggested it is unconformable (Moore, 1997; Heydari and Baria, 2005). However, this discrepancy may be related to local variations in subsidence between basins and salt movement (Dickinson 1969; Wilkinson, 1984; Ewing, 2009;). The Buckner Anhydrite was deposited in a broad intrashelf lagoon that was cut off from open-ocean circulation by Gilmer sediments at the shelf edge (Stewart, 1984; Moore et al., 1988). Further downdip into the paleo-GOM Basin, the Gilmer limestone transitions into the Gilmer shale (Fig. 5). During Haynesville deposition salt movement is interpreted as being most active (Wilkinson, 1984). This activity produced areas of localized subsidence and mini-basins from salt withdrawal. Concurrently, salt diapirs and pillows formed high-relief structures and anticlinal features. (Seni and Jackson, 1983). These high-relief structures created nucleation sites for shallow-water, high-energy sand shoals (grainstone) development (Wilkinson, 1984).

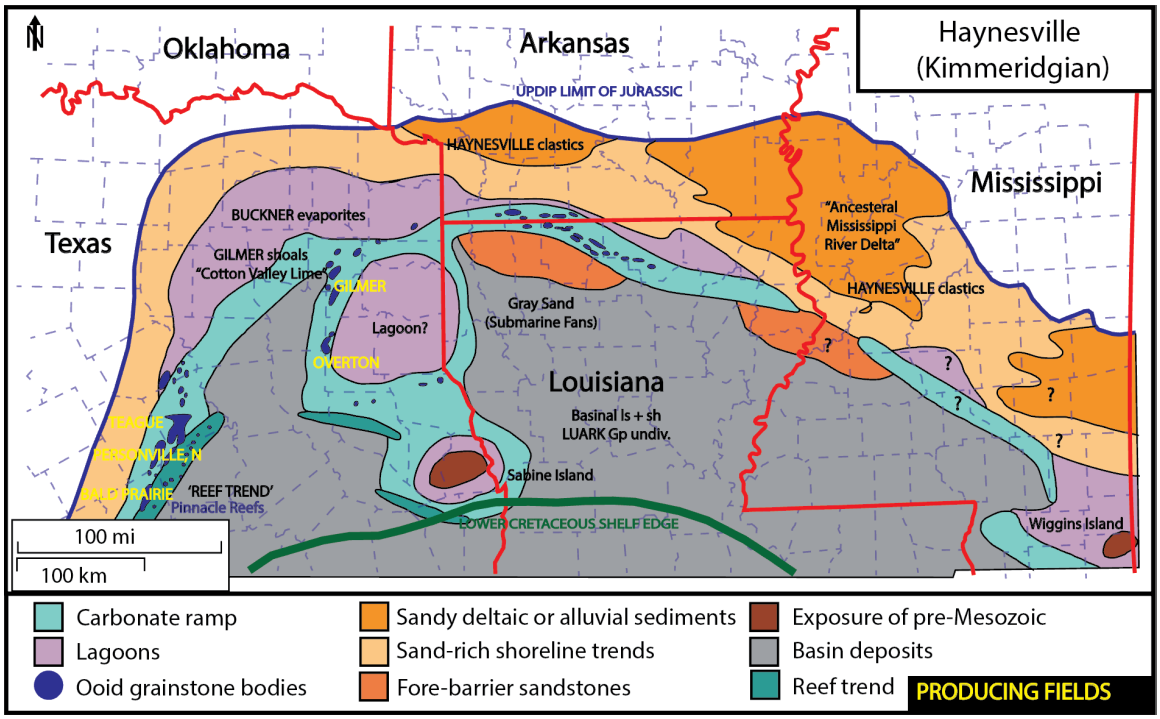

Figure 5 Map of depositional systems of the Haynesville along the northern Gulf of Mexico during the Kimmeridgian time period. Modified after Ewing (2001).

CHAPTER 3: DATA AND METHODS

A single core (713 ft) was used in this study, from the Sun Travis GU No. 1 well in Van Zandt County, Texas. The core was slabbed and etched with hydrochloric acid. The slabbed core was described using a binocular scope and with aid of thin sections impregnated with blue visible epoxy and blue fluorescence dye. The description procedure followed the methodology outlined in Bebout and Loucks (1984) and lithofacies were in-part named using Dunham's textural classification (Dunham, 1962). A total of 87 sections (50 x 75 mm) were used to define depositional texture, mineralogy, and allochem content with a petrographic microscope. Geochemical analysis of the core was done using the following methods; total organic carbon (TOC) and Rock-Eval, x-ray diffraction analysis (XRD), x-ray fluorescence (XRF) analysis, inorganic and organic carbon isotope analysis, and oxygen isotope analysis.

A total of 28 samples were taken for Leco TOC and Rock-Eval analysis. The Leco TOC analysis was run on a LECO C230 instrument and the Rock-Eval analysis was run on a Rock-Eval II instrument.

Energy-dispersive x-ray fluorescent (XRF) data was performed at two-inch intervals along the full extent of the core for 10 major elements and 20 trace elements generating 107,520 data points. The XRF analysis was completed using a Bruker AXS Tracer III-V XRF handheld unit. The unit was calibrated for both major and trace analysis using methodology outlined by Rowe et al (2012). The core was scanned for

major elements using 15 kV for 60 seconds and for trace elements using 40 kV for 90 seconds.

For semi-quantitative XRD analysis 14 samples were taken and analyzed by K-T Geoservices in Gunnison, CO. The analysis was performed using a Siemens D500 automated powder diffractometer equipped with a copper X-ray source (40kV, 30mA) and a scintillation X-ray detector.

For organic carbon, inorganic carbon, and oxygen isotope analyses, 307 bulk rock samples were taken along the extent of the 592 ft Smackover interval of the core. Samples were drilled every 3 ft and at points with relatively high XRF readings for Ca, Mg, Si, Al, and Sr in order to sample a range of lithology types. Powdered samples were drilled from the back of the core. Inorganic carbon ($\delta^{13}C_{VPDB}$) and oxygen ($\delta^{18}O_{VPDB}$) samples were run on a ThermoElectron Gas Bench II and a Delta V continuous flow isotope ratio mass spectrometer (IRMS) at the Bureau of Economic Geology, The University of Texas at Austin. Carbon and oxygen isotope calibration curves were generated using replicate analyses of the internationally distributed standards NBS-19 ($\delta^{13}C_{VPDB}$ = +1.95‰ $\delta^{18}O_{VPDB}$ = -2.20‰) and NBS-18 ($\delta^{13}C_{VPDB}$ = -5.014‰ and $\delta^{18}O_{VPDB}$ = -23.2‰). Organic carbon isotope ($\delta^{13}C_{VPDB}$) samples were pretreated for the removal of inorganic carbon using the methods outlined by Larson et al. (2008) and were analyzed using a Costech elemental analyzer (EA) coupled to a Thermo Electron Delta V continuous flow isotope ratio mass spectrometer (IRMS) at the Bureau of Economic Geology, The University of Texas at Austin. A carbon isotope calibration curve was

generated using analyses of the internationally distributed standards USGS24 ($\delta^{13}C_{VPDB}$ = -16.05‰), IAEA-C5 ($\delta^{13}C_{VPDB}$ = -25.49‰), and IAEA CH-7 ($\delta^{13}C_{VPDB}$ = -32.15‰).

CHAPTER 4: LITHOFACIES

Introduction to Lithofacies

The complete core description for the Smackover and Buckner sections in the Travis GU No.1 core is presented in Figure 6. Ten lithofacies were differentiated on the basis of the carbonate texture classification of Dunham (1962). Lithofacies were defined by texture, biotas, mineralogy, and sedimentological and biological features. Mineralogical changes and fossil types and abundances were recorded. In some sections of the core, dolomitization and anhydrite replacement obscure the rock fabric. Alongside the core description is a plot showing the XRF measured relative elemental abundances of Ca, Mg, Si, Al, and S which are proxies of calcite, dolomite, and anhydrite (Ca), Dolomite (Mg), quartz, feldspar, and clay (Si), clay (Al), and pyrite and anhydrite (S).

The Smackover section in East Texas is made up of three informal members the upper, middle, and lower Smackover. The lithofacies identified in this core further subdivide the Smackover units into recognizable packages and these packages correspond to depositional environment. The depositional setting of the Smackover Formation in Texas, Arkansas, and Louisiana has been well documented as a ramp setting (Ahr, 1973; Budd and Loucks, 1981; Ewing, 2001; Heydari and Baria, 2005). This investigation also recognizes a ramp system for the Smackover section in the Travis GU No. 1 core as will be discussed below. Therefore, the lithofacies are presented in context of this depositional model.

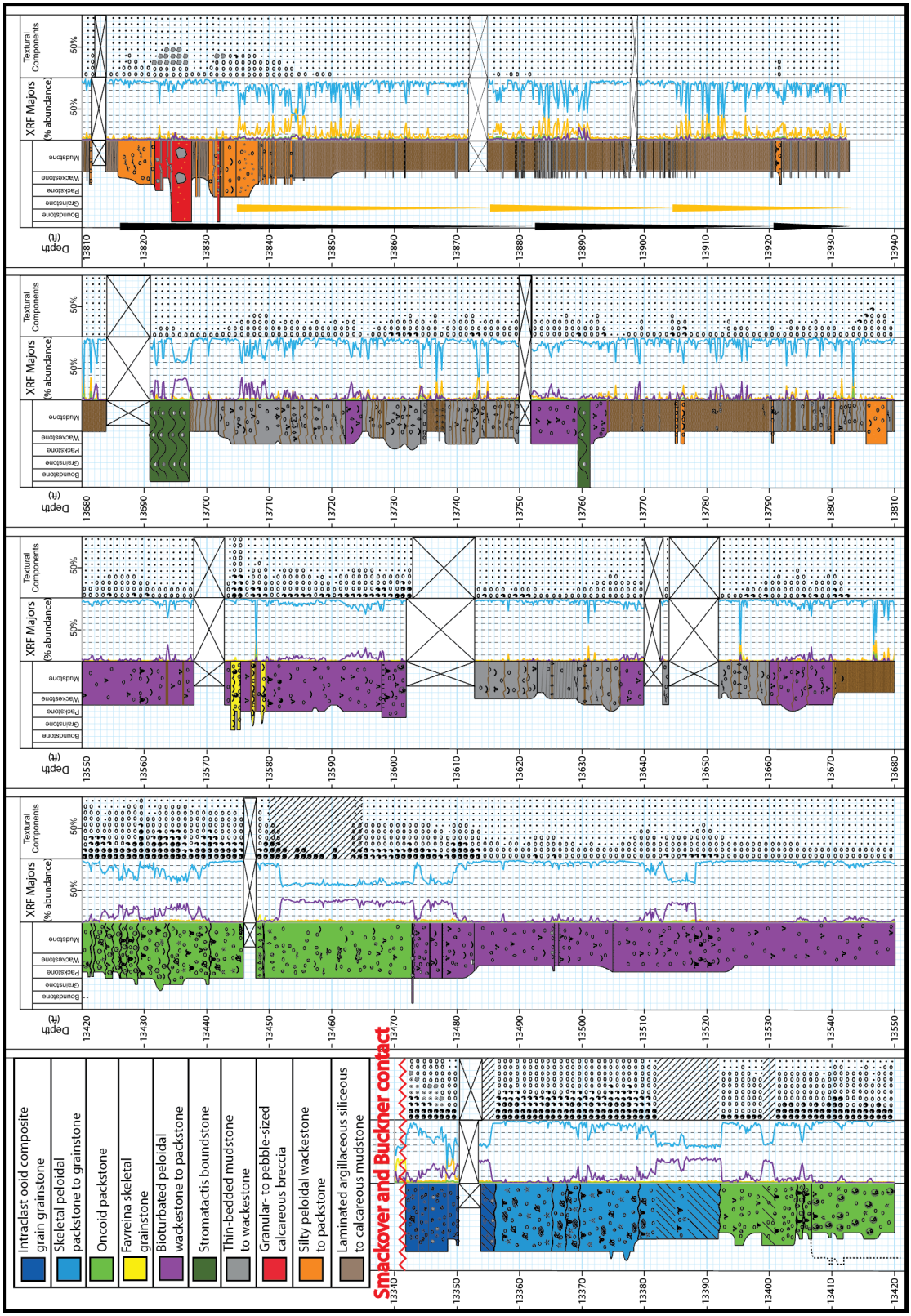
Intraclast ooid composite grain grainstone
Skeletal peloidal packstone to grainstone
Oncoid packstone
Favreina skeletal grainstone
Bioturbated peloidal wackestone to packstone
Stromatactis boundstone
Thin-bedded mudstone to wackestone
Granular- to pebble-sized calcareous breccia
Silty peloidal wackestone to packstone
Laminated argillaceous siliceous to calcareous mudstone
Smackover and Buckner contact
Depth (ft)
XRF Majors (% abundance)
Textural Components
50%
Boundstone
Grainstone
Packstone
Wackestone
Mudstone

Figure 6.

Figure 6: Travis Gas Unit No.1 well core description. Refer to Figure 14 for the legend of features and lithofacies described. For the XRF column, the curves displayed are silica in orange, sulfur in yellow, aluminum in green, magnesium in purple, and calcium in blue. Black and Yellow wedges highlight potential cyclic trends in bundled gravity flows and silica content respectively.

Lower Smackover Formation Lithofacies

LAMINATED ARGILLACEOUS TO CALCAREOUS MUDSTONE (LAMINATED MUDSTONE)

Description: The lithofacies is composed of three distinct bedding styles; millimeter-scale laminae of quartz silt and organic-rich layers (Fig. 7E), millimeter- to a centimeter-scale carbonate-rich laminae (Fig. 7F), and thin bedded carbonate muds (Fig. 7A). The quartz silt and organic-rich laminae alternate with the carbonate-rich laminae at the scale of several laminae to thin packages that are cm's thick. Some laminate pinch out and laterally transition between the different types (Fig. 7D). Vertical contacts between laminae are non-gradational and abrupt. The carbonate-rich laminae are generally capped by parallel and continuous layers of quartz silt (Fig. 7F) and in some cases, higher up in the cores section, *Favreina* pellets (shrimp pellets). The laminated beds show several features including planar lamination, wavy lamination, discontinuous disrupted lamination, low-angle ripple cross-laminations, and small-scale compression structures such as small folds and millimeter-scale faults (Fig. 7B). Within the laminated organic matter micro-folding is observed (overturned bacterial mat) (Fig. 7C). The laminated intervals contain an abundance of small pyrite framboids, ranging 2 to 20 microns in size, that are observed replacing organics (Fig. 8 E, F). In the upper section (above 13790 ft) pyrite becomes less abundant and possible concretions are observed. The thin bedded carbonate mudstones range in thickness from 3 cm to 16 cm and form abrupt contacts with the laminated layers. These beds commonly contain fining upwards sequences and

current and traction hydrodynamic features such as peloid lags, ripples, and scour surfaces as well as current related laminations (Fig. 7A).

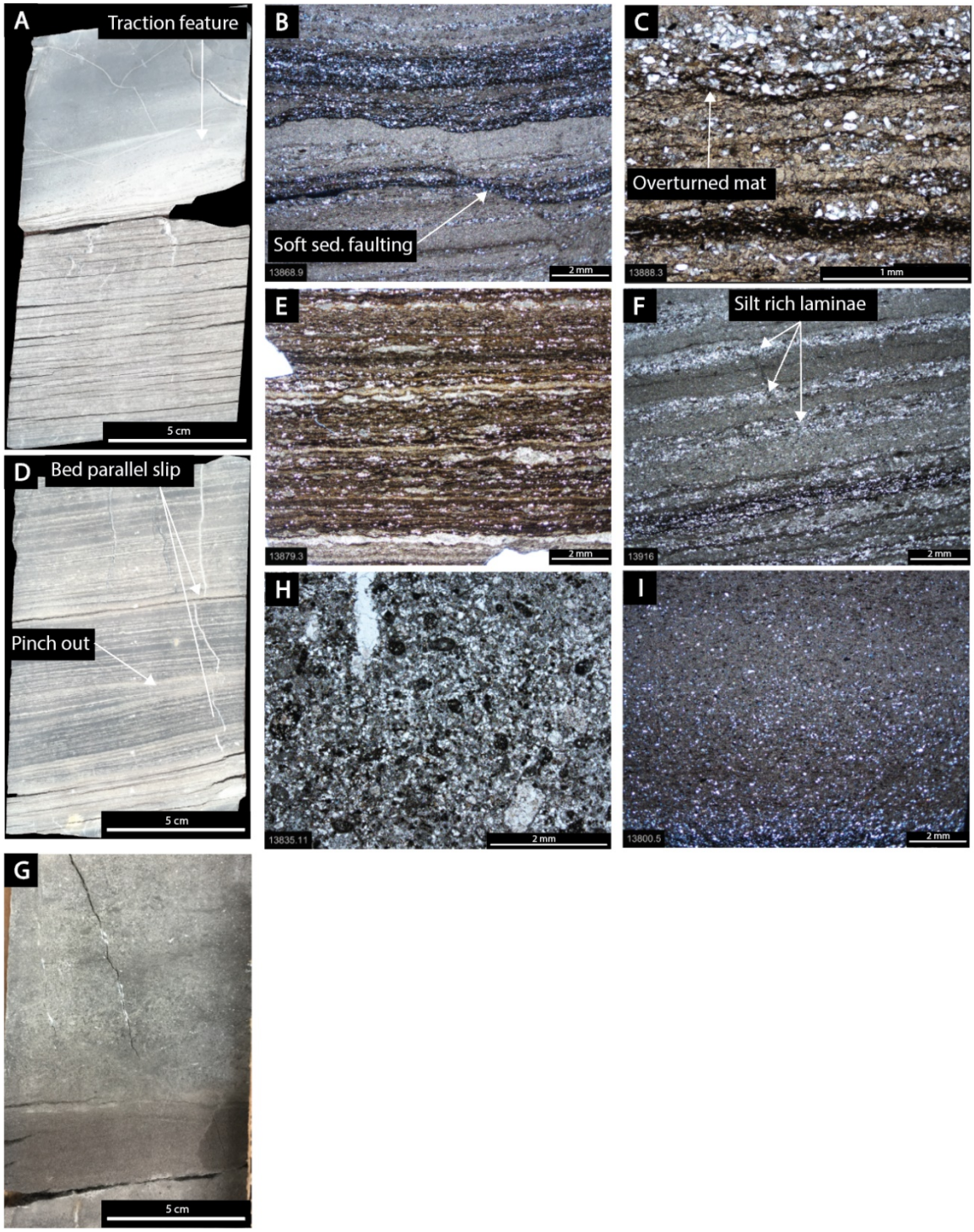
A
Traction feature
5 cm
B
Soft sed. faulting
13868.9
2 mm
C
Overturned mat
13888.3
1 mm
D
Bed parallel slip
Pinch out
5 cm
E
13879.3
2 mm
F
Silt rich laminae
13916
2 mm
G
5 cm
H
13835.11
2 mm
I
13800.5
2 mm

Figure 7.

Figure 7. Photographs A through F were taken from the laminated argillaceous siliciclastic to calcareous mudstone lithofacies and G through H were taken from the silty peloidal wackestone to packstone lithofacies. (A) Thin-bedded mudstone with basal traction feature overlying quartz silt and organics-rich laminae. (B) Organic matter and silt-rich laminae underlying laminated calcareous mudstone with soft-sediment faulting. (C) Overturned bacterial mat. (D) Carbonate-rich laminae and quartz silt-rich laminae interbedded. Carbonate laminae pinching out, Fractures concentrated in carbonate-rich beds, and fractures altered by bed parallel slip. (E) Organic-matter-rich set of laminated muds. (F) Carbonate-rich laminae capped by quartz silt-rich laminae. (G) Silty peloidal packstone lithofacies, darker colored portion of the core contains more silt and the light portion being more carbonate- and peloid-rich. (H) Quartz grains and peloids suspended in a carbonate mud matrix. (I) Quartz silt and peloid grains fining upwards (less quart silt-rich) within a carbonate mud matrix.

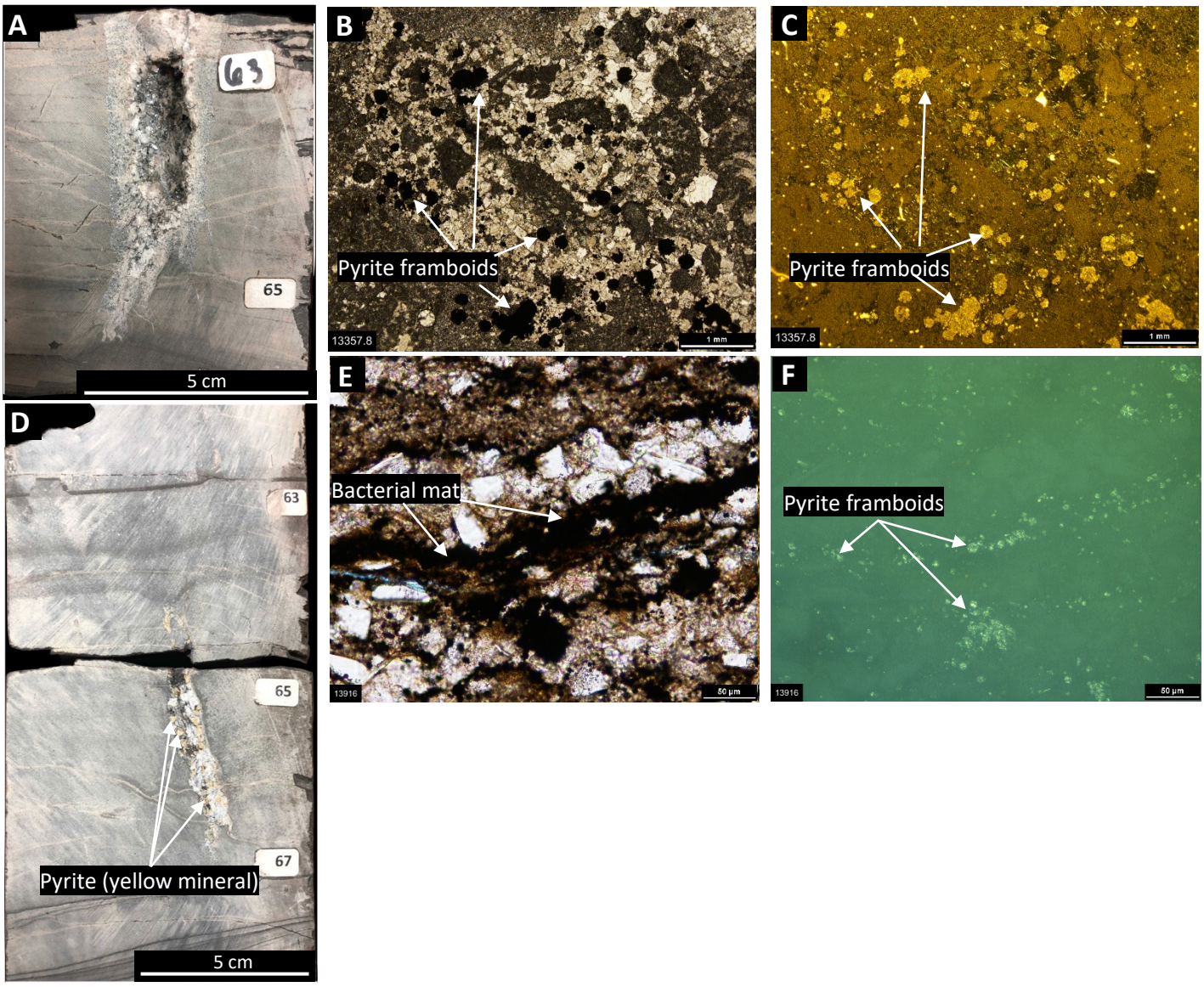

Figure 8: Photographs A through F show the various occurrences of pyrite. (A) Large open fracture vug filling with dolomite and sulfide minerals. (B) Large pyrite framboids (opaque minerals) filling intercrystalline pore space. (C) Same image as B but reflected light. Gold minerals are pyrite framboids. (D) Large closed fracture filled with pyrite (yellow minerals) and dolomite. (E) Bacterial mat organics (opaque) in the lower laminated mudstone lithofacies. (F) Same image as E but reflected light. Light specs are pyrite framboids replacing organics.

There are abundant fractures ranging from 1 mm to 2.5 cm wide and 3 cm to 15 cm long and are confined to the more carbonate-rich intervals. Some fractures are filled by coarse crystalline calcite and dolomite cement (Fig. 8A, D). Most of the fractures are wavy ptygmatic fractures, meaning they formed during early compaction, and some have been altered by bed parallel slip (Fig. 7D). Additionally, injection features of carbonate poor muds filling early formed fractures in carbonate beds are common. These features contain calcareous siliciclastic muds partially filling or fully filling in fractured hinges created by rotated beds. Bedding angle changes are also observed in this interval, some are subtle changes and others extreme and accompanied by fragmented bedding.

Interpretation: Preservation of laminations, little to no bioturbation, pyrite framboids, and lack of benthic organisms indicates the environment of deposition was in a low-energy distal anoxic setting. Additionally, there is a lack of fossils and peloids from organisms living within the water column, aside from minor amounts of *Favreina* pellets transported from shallower settings by gravity flows, which indicates the water column may have been stressed, potentially as a result of elevated salinities. The organics that are interlaminated with the carbonate muds and quartz silt are interpreted as being formed by sulfur reducing bacterial mats. This interpretation is based on the observations of continuous and parallel laminae, overturned mats, and geomarker studies discussed in the literature (Claypool and Mancini, 1989; Sassen, 1990) for other lower Smackover sections. This interpretation is similar to those made by Budd and Loucks (1981) in South Texas, Heydari et al. (1997) in Arkansas and Mississippi, Moore (1997) in Southern Arkansas, and Harwood and Fontana (1983) in East Texas. Other authors have

interpreted the laminated muds as lagoonal algal mats deposited in shallow-water settings (Malek-Aslani, 1973; Mitchell-Tapping, 1984; Hancharik, 1984). However, this interpretation is considered incorrect for the lower Smackover section in this core because of the lack of burrows and shallow-water skeletal grains, features that are expected to be present in a shallow quiet-water setting where lagoonal algal mats could develop (Shinn, 1983). The quartz grains present in the parallel and continuous laminae are interpreted to have been terrigenous sourced possibly by aeolian windblown dust that settled out of the water column onto the substrate. This interpretation is based on the well-sorted silt-sized character of the grains as well as the proximity of aeolian environments along the paleo-coastline (Budd and Loucks, 1981).

Thin-bedded carbonate mudstones are interpreted as mud-rich gravity flow deposits because of the presence of traction features and fining upward sequences with high concentrations of quartz silt at the base of the mud packages. Additionally, the presence of early fracturing, bed parallel slip and injection of un-lithified muds into early fractured compacted carbonate beds indicates that there was instability of the substrate after deposition possibly due to salt tectonics or a lack of early cementation.

SILTY PELOIDAL WACKESTONE TO PACKSTONE

Description: This lithofacies is composed of *Favreina* pellets and quartz silt within a carbonate mud matrix (Fig. 7G). Beds are typically structureless or contain fining-upward grading and are 5 cm to a 30 cm thick with some beds that are 1 m to 2 m thick. Most packages are made up of quartz silt (mud- to grain-supported), clay material, and peloids

(Fig. 7H). Some beds have minor amounts of mollusk fragments and calcite-filled small molds. The lithofacies is generally bounded above and below by dark argillaceous and silt-rich dissolution seams. Some intervals contain enhanced porosity possibly related to dissolution of carbonate material (Fig. 7I).

Interpretation: Presence of coarser grains relative to the vertically adjacent lithofacies and fining upward sequences indicate the silty peloidal wackestone to packstone matrix was deposited by episodic gravity flow events. These events were probably mud-rich gravity flows that, as they traveled down the ramp, incorporated debris that settled out of the water column onto the substrate.

Granular- to Pebble-Sized Calcareous Breccia

Description: This lithofacies is made up of poorly sorted angular clasts supported by a silty peloidal wackestone to packstone matrix (Fig. 9A). The intraclasts are composed of laminated mudstones, silty peloidal wackestone to packstones, and occasionally eroded algal mat material (Fig. 9B, C). Below and above the lithofacies there is an abundance of broken up bedding, soft sediment deformation and injection features.

Interpretation: This lithofacies is interpreted as debris flow deposits based on the clasts supported by matrix and erosion and incorporation of underlying material (Fig. 9B, C).

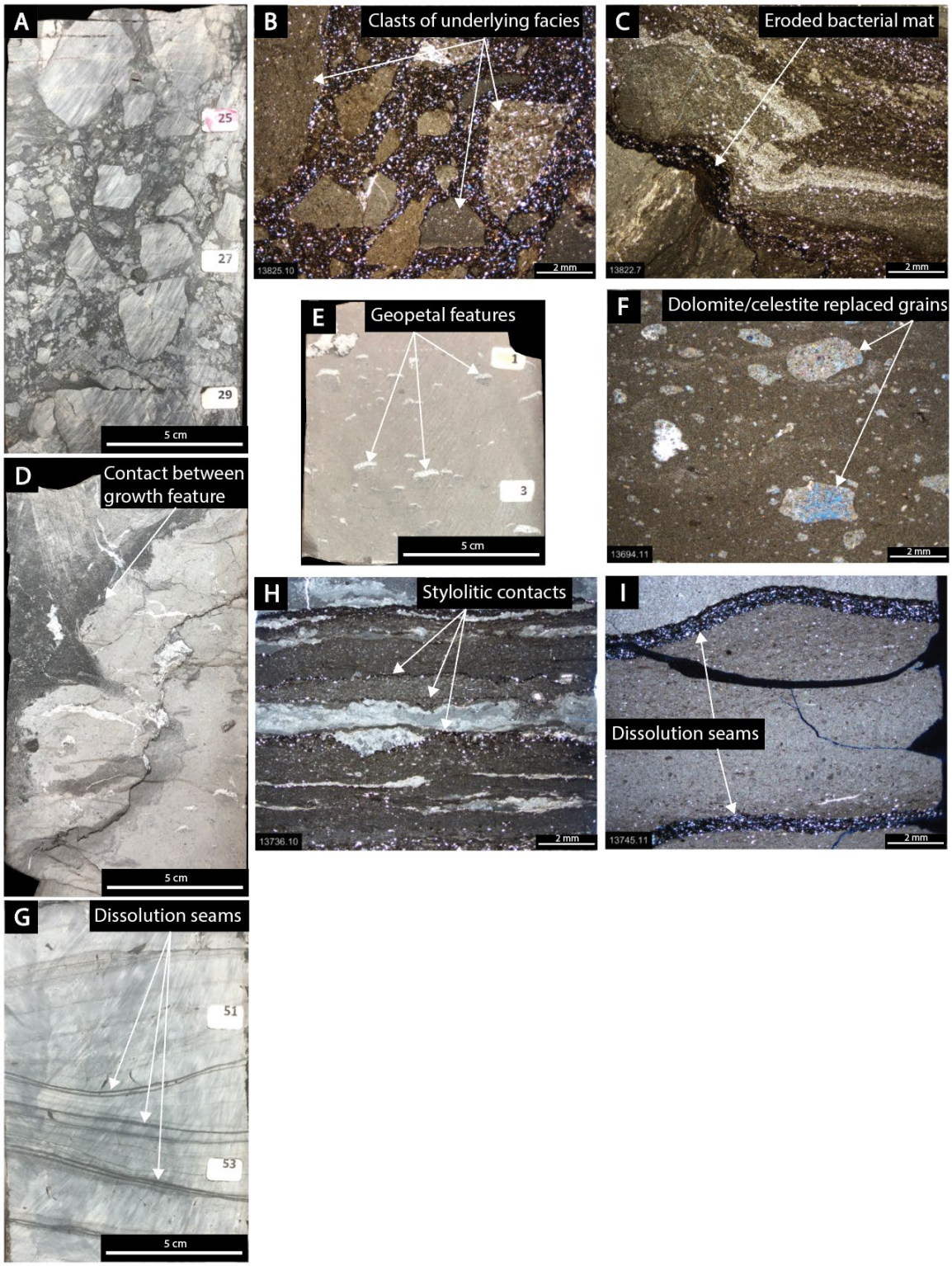
A
25
27
29
5 cm
B
Clasts of underlying facies
13825.10
2 mm
C
Eroded bacterial mat
13822.7
2 mm
D
Contact between growth feature
5 cm
E
Geopetal features
1
3
5 cm
F
Dolomite/celestite replaced grains
13694.11
2 mm
G
Dissolution seams
51
53
5 cm
H
Stylolitic contacts
13736.10
2 mm
I
Dissolution seams
13745.11
2 mm

Figure 9.

Figure 9: Photographs A through C were taken from the granular to pebble calcareous breccia lithofacies, D through F were taken from the stromatactis boundstone lithofacies, and G through I are from the thin-bedded mudstone to wackestone lithofacies (A) Mudstone clasts supported by matrix. (B) Mudstone to wackestone clasts suspended in a quartz-silt and mud-rich matrix. (C) Deformation and breakage of bedding and transport of organic-rich bacterial mat. (D) Contact between stromatactis (light colored) and surrounding sediment (dark colored), heavily fractured. (E) geopetal vugs in stromatactis. (F) Clasts replaced by dolomite and celestite (blue mineral). (G) Carbonate mudstones separated by dissolution seams. (H) Thin-bedded mudstones and wackestones separated by solution seams. (I) Fining upward sequence with “coffee ground organics” at the top and dissolution seams bounding the thin bed on top and bottom.

THIN-BEDDED MUDSTONE TO WACKESTONE

Description: This lithofacies is made up of thinly bedded mudstones to wackestones that are separated from one another by wavy organic- quartz-silt- and argillaceous- rich dissolution seams (Fig. 9G, I). The mudstone to wackestones commonly contain fining-upward textures and peloidal lags (Fig. 9I). The amount of peloids and skeletal fragments within the lithofacies increases up section. Additionally, there is an increase in soft-sediment deformation, abruptly truncated bioturbated intervals, and diagenetic alteration by dolomite and celestine up section as well. The zones of dissolution seams range in thickness from mm's to 10's of cm's and are commonly surrounded by diagenetic alteration halos (Fig. 9H, I). The dissolution seams contain elevated TOC's, up to 1.59 wt%, and can contain celestine crystals within the seam.

Interpretation: These thin beds are made up of stacked packages that contain similar traction and fining upward textures to the thin-bedded mudstones within the lower laminated mudstone interval. The stacking of these beds indicates multiple phases in which these flows were being deposited. The dissolution seams formed during early burial diagenesis and probably concentrated insoluble material such as quartz-silt, clay minerals, and organic matter that accumulated during periods of low energy and waning current. These seams form the contact between the carbonate mudstone beds. The

thickness of these seams may relate to the amount of time or the amount of insoluble material accumulated between mud flow events.

STROMATACTIS BOUNDSTONE

Description: This lithofacies is composed of a fabric that has been heavily replaced with fine-crystalline dolomite. The fabric is mud-dominated with peloids supported by the finer mud matrix. It contains abundant, laterally elongated cavities with geopetal sediment at the base and the upper part of the cavity filled by equant coarse-crystalline dolomite (Fig. 9E). Some clasts are replaced by dolomite and celestine (Fig. 9F). The lithofacies contains growth features that produce angular contacts with the intervening mud (Fig. 8D). Along these contacts there are an abundance of intraclasts suspended within the lighter colored boundstone lithofacies.

Interpretation: Diagenetic alteration and a cryptic rock fabric cause there to be some uncertainty in the interpretation of this lithofacies. The cavities resemble potential forms of "stromatactis" that are associated with mud mounds that may have an organic or inorganic origin (Flugel, 2004, p. 194). Additionally, the incorporation of peloidal material within the mud mound matrix and intraclasts at the edges of the mounds are commonly associated with stromatactis growth (Matyszkiewics, 1993). Because of the extensive dolomitization of this lithofacies little criteria is available to provide an exact origin for the potential buildups.

Middle Smackover Formation Lithofacies

BIOTURBATED PELOIDAL WACKESTONE TO PACKSTONE

Description: This lithofacies is composed of bioturbated wackestone to packstones containing abundant peloids, *Favreina* pellets and skeletal fragments (Fig. 10C). The skeletal material within the lithofacies is mostly thin-walled mollusks, echinoderm fragments, and oyster fragments. Some algal-coated skeletal grains are also present and are most common up section. Peloid grains and matrix material within burrows have been preferentially replaced by dolomite (Fig. 10B). The lithofacies also contains abundant clay-rich, horse-tail dissolution seams and stylolites (Fig. 10A). Firm grounds are also observed as abrupt boundaries commonly associated with eroded rip-up clasts above or sediment filled burrows below. These surfaces become more common up section as the bioturbated lithofacies transitions into the oncoid packstone lithofacies.

Interpretation: Based on the abundance of mud and bioturbation, this lithofacies represents a low-energy, quiet-water setting with oxygenated bottom-sediment and -water conditions. Oxygenated bottom water allowed organisms to live at the sediment-water interface where they reworked the sediment and their skeletal remains and peloids contributed to the sediment mass. Burrowing may have destroyed any previous sedimentary structures, but the abundance of mud matrix indicates deposition under low-energy conditions. This interpretation is similar to that of (Budd and Loucks, 1981; Harwood and Fontana, 1983) for the same lithofacies in East Texas and South Texas respectively.

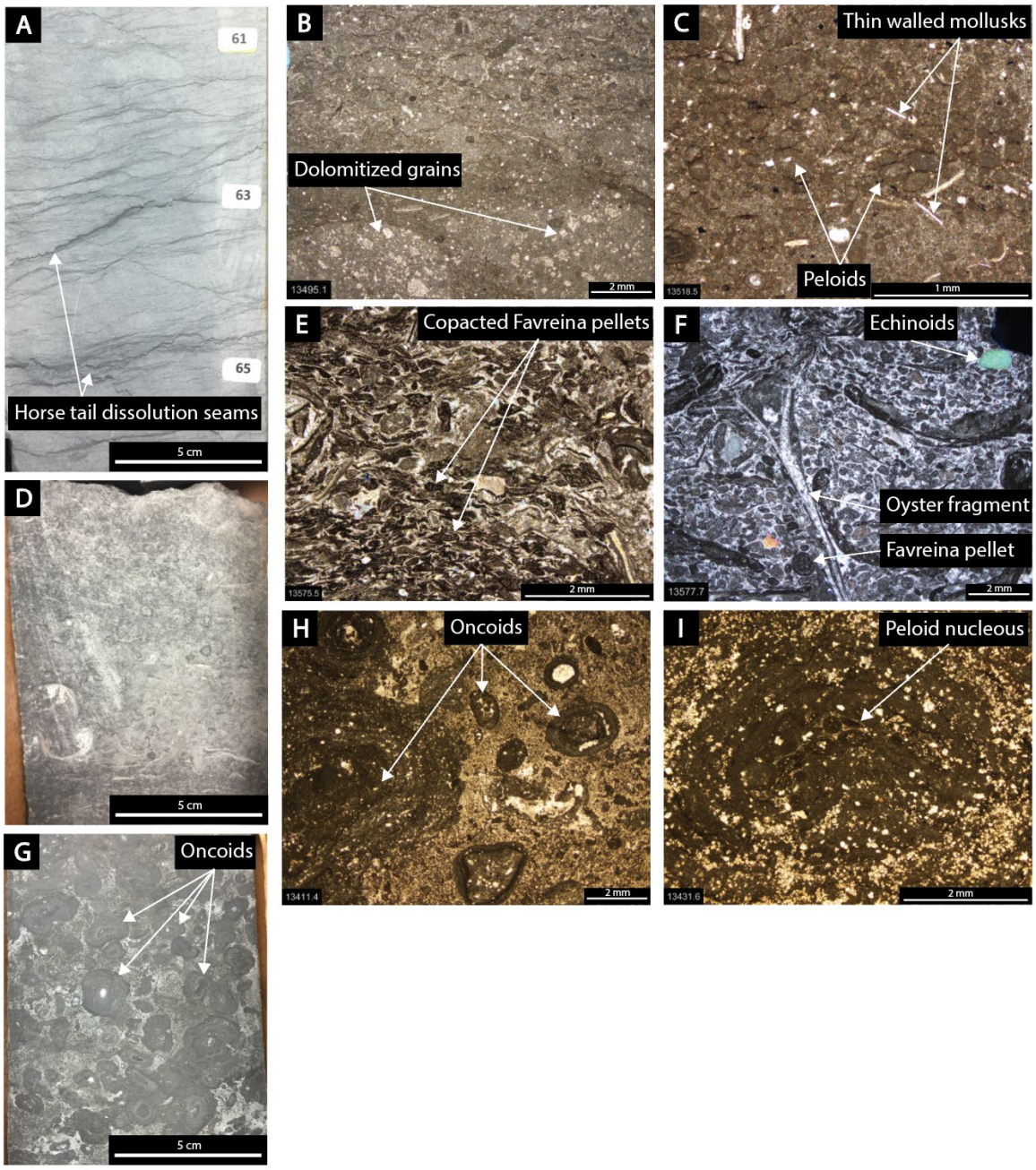
A
61
63
65
Horse tail dissolution seams
5 cm
B
Dolomitized grains
13495.1
2 mm
C
Thin walled mollusks
Peloids
13518.5
1 mm
D
5 cm
E
Copacted Favreina pellets
13575.5
2 mm
F
Echinoids
Oyster fragment
Favreina pellet
13577.7
2 mm
G
Oncoids
5 cm
H
Oncoids
13411.4
2 mm
I
Peloid nucleous
13431.6
2 mm

Figure 10.

Figure 10: Photographs A through C were taken from the bioturbated peloidal wackestone to packstone lithofacies, D through F from the *Favreina* skeletal grainstone lithofacies, and G through I from the oncoid packstone lithofacies. (A) Bioturbated sediment with abundant horse-tail-dissolution seams. (B) Dolomitized burrows in a wackestone matrix. (C) Peloids and thin-walled mollusks within a dominantly mud matrix. (D) Massive grainstone (E) Compacted *Favreina* pellets. (F) Grainstone with algally coated grains, echinoids, *Favreina* pellets, and mollusk fragments. (G) Oncolite rudstone with anhydrite replacing some nuclei. (H) Oncolites with various types of nuclei in a dolomitized matrix. (I) Oncoid with a group of peloids as the nuclei being dolomitized.

FAVREINA SKELETAL GRAINSTONE

Description: This lithofacies is composed of three grainstone intervals containing skeletal fragments and *Favreina* pellets (Fig. 10D). The grains include mollusks, echinoderms, and oyster fragments, of which most are coated with algae (Fig. 10F). The grains have undergone physical compaction resulting in broken skeletal material and ductile compacted *Favreina* pellets (Fig. 10E). The three intervals have varying degrees of sorting, mud content, and skeletal fragments and are interbedded with the bioturbated peloidal wackestone to packstone lithofacies separated by abrupt dissolution seam or stylolitic contacts.

Interpretation: This lithofacies suggest gravity flow deposition in the middle ramp that originated in the up-dip inner ramp. This interpretation is based on the abundance of shallow-water grains and because the lithofacies appears abruptly in contrast to no significant change in the depositional styles of the surrounding lithofacies.

Upper Smackover Formation Lithofacies

ONCOID PACKSTONE

Description: The oncoids packstone lithofacies is composed of algal coated peloidal and skeletal grains (Fig. 10H, I). The fabric is predominantly packstones and grainstones, but in some sections floatstones and rudstones, depending on the size of the oncoids. The sizes vary from 0.3 mm to over 20 mm in diameter and their nucleus is

commonly replaced by anhydrite (Fig. 10G). The fabric is generally bimodal with oncoid grains suspended in a dolomitized clotted peloidal packstone with variable amounts of skeletal fragments (Fig. 10H, I). The skeletal grains are mostly thin walled mollusks, echinoids, and oyster fragments. Most skeletal grains, including rip-up clasts and peloids have some amount of algal coating.

Portions of the lithofacies contain many cycles of firm grounds (possibly some are hardgrounds) with sediment-filled burrows, overlain by rip-up clasts and a fining upward sequence of former sediment (Fig. 11A). Other portions of the lithofacies have been heavily altered by fabric destructive coarse-crystalline dolomite. These dolomitized intervals have abundant intercrystalline pore space and commonly have anhydrite crystals and nodules present. Within the intercrystalline pore spaces there is solid bitumen and large (50 to 300 microns) pyrite framboids.

Interpretation: Diagenetic alteration of the lithofacies makes it difficult to fully understand. The lithofacies make-up of oncoids and algally coated grains signifies deposition in an environment within the photic zone with periodic agitation of grains yet still low-energy based on the abundance of muds. Periodic agitation was probably caused by storm-related currents or agitation. Erosion of the bottom sediments was likely during high-energy storm events and the mobilized sediment filled burrows below the firm ground and waning currents deposited fining upward sequence above the firm ground. The variation in oncoid sizes and sediment structures within the oncoids packstone lithofacies may suggest a broad range of physical processes in this environment of deposition.

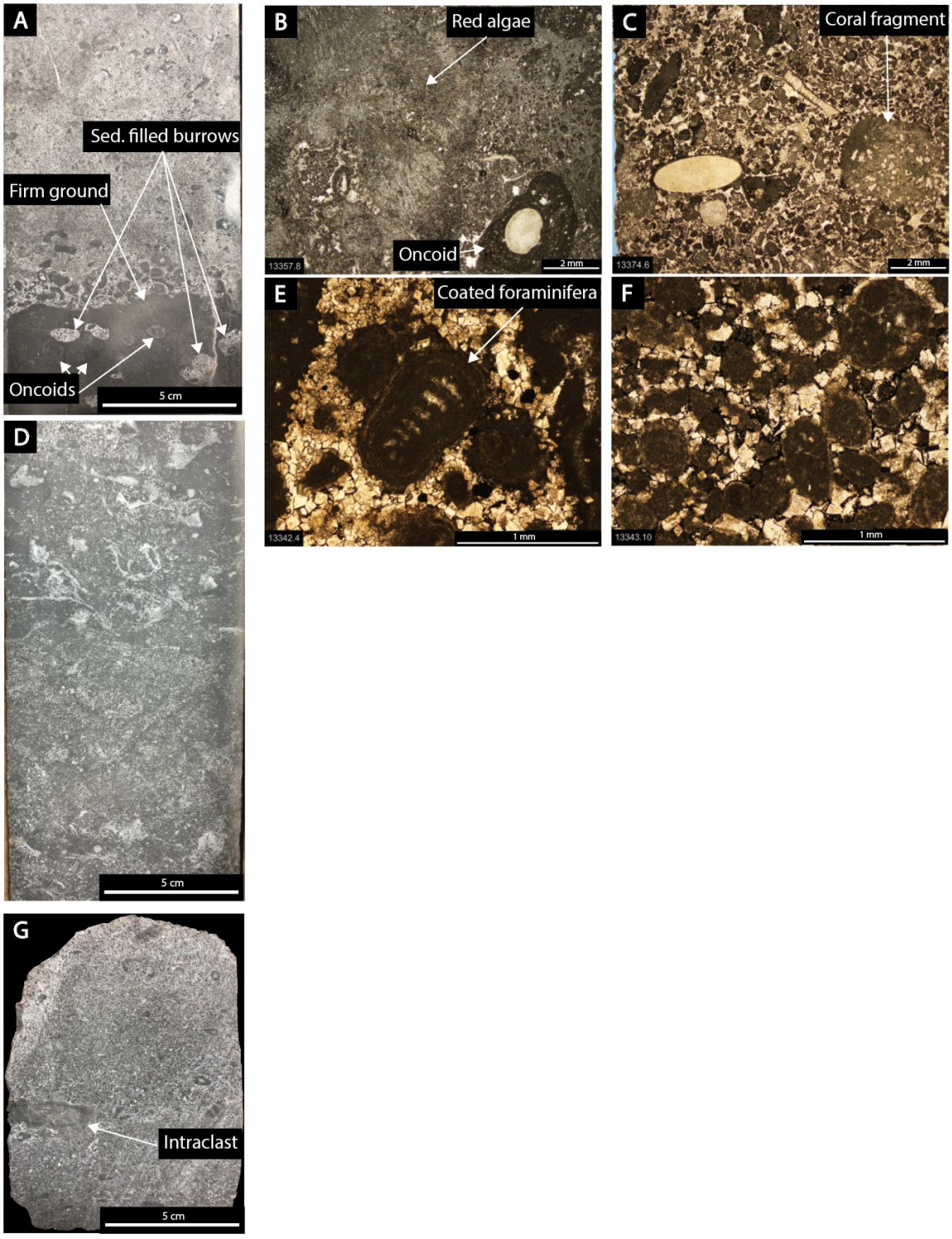
A
Sed. filled burrows
Firm ground
Oncoids
5 cm
B
Red algae
Oncoid
13357.8
2 mm
C
Coral fragment
13374.6
2 mm
D
5 cm
E
Coated foraminifera
13342.4
1 mm
F
13343.10
1 mm
G
Intraclast
5 cm

Figure 11.

Figure 11: Photograph A was taken of the oncoid packstone, B through D from the skeletal peloidal packstone to grainstone lithofacies, and E through G from the intraclast ooid composite-grain grainstone lithofacies. (A) Firm ground with sediment filled burrows, overlain by rip-up clasts and a fining upward sequence (B) Red algae fragment and algally coated echinoid fragment. (C) Skeletals and peloids with dolomitized interparticle pore space, coral fragment present. (D) Skeletal-rich grainstone. E) Coated skeletal grain that has been micritized in a heavily dolomitized matrix. (F) Heavily micritized grapestones, peloids, and ooids within a dolomitized matrix, solid bitumen filling intracrystalline pore space. (G) Moderate to well-sorted grainstone with large intraclast.

Skeletal Peloidal Packstone to Grainstone

Description: The skeletal peloidal packstone to grainstone lithofacies is primarily made up of skeletal fragments and peloids within a generally dolomitized matrix (Fig. 11C, D). The skeletal grains are mollusks, echinoids, corals, and red algae and most grains have some extent of algal coating (Fig. 11B). The lithofacies also contains various types and sizes of peloids. The smaller sized peloids form a clotted peloidal matrix fabric and larger peloids, such as *Favreina* pellets are larger grains. Most grains other than echinoid and mollusk fragments have been heavily micritized, with some being difficult to distinguish. Multiple firm grounds showing erosion or truncated grains are present. Some burrows are also present and are highlighted by dolomitization.

Interpretation: The lithofacies is grain-rich but poorly sorted so it was likely deposited in a moderate to high-energy setting within the fair-weather-wave base. The variety of grain types indicates this environment was occupied by a diverse assemblage of organisms and deposited in marine waters that were well-oxygenated and of normal salinity.

Intraclast Ooid Composite Grain Grainstone

Description: This lithofacies has been heavily altered by fabric destructive dolomitization and micritization of grains making it difficult to describe. It is composed of intraclasts, micritized grapestones, ooids, and rhodoliths (Fig. 11G, E, F). The

lithofacies contains intraclasts-rich grainstones that fine upwards into well-sorted grain dominated packstones as well as an interval with faint cross laminations. The top of the lithofacies forming the contact between the Smackover Formation and the overlying Buckner Anhydrite is an erosional surface showing signs calichefication (Fig. 13A). The base of the lithofacies is an erosional contact and is heavily dolomitized, has higher porosity, and contains abundant vugs.

Interpretation: Because of the heavy diagenetic alteration of the lithofacies there is some uncertainty in grain types and textures. However, it appears that the lithofacies may shoal upwards and contain ooid grains which would suggest shallow-water deposition in an environment with constant wave agitation such as an ooid shoal.

Buckner Anhydrite Lithofacies

The Buckner section of the core (Fig. 12) is composed of predominantly anhydrite and interbedded sandstones (13342 ft to 13220 ft). The anhydrite may have been original depositional anhydrite or gypsum transformed to anhydrite as a result of dehydration during burial. As gypsum changes to anhydrite there is a decrease in volume which may cause original depositional features to be altered, deformed or completely obliterated (Mann and Kopaska-Merkel, 1992). Additionally, it is thought that the Louann Salt was active during and after Buckner deposition which led to tectonic deformation of the anhydrite units (Wilkinson, 1984). These factors obscure some of the depositional detail of the Buckner section.

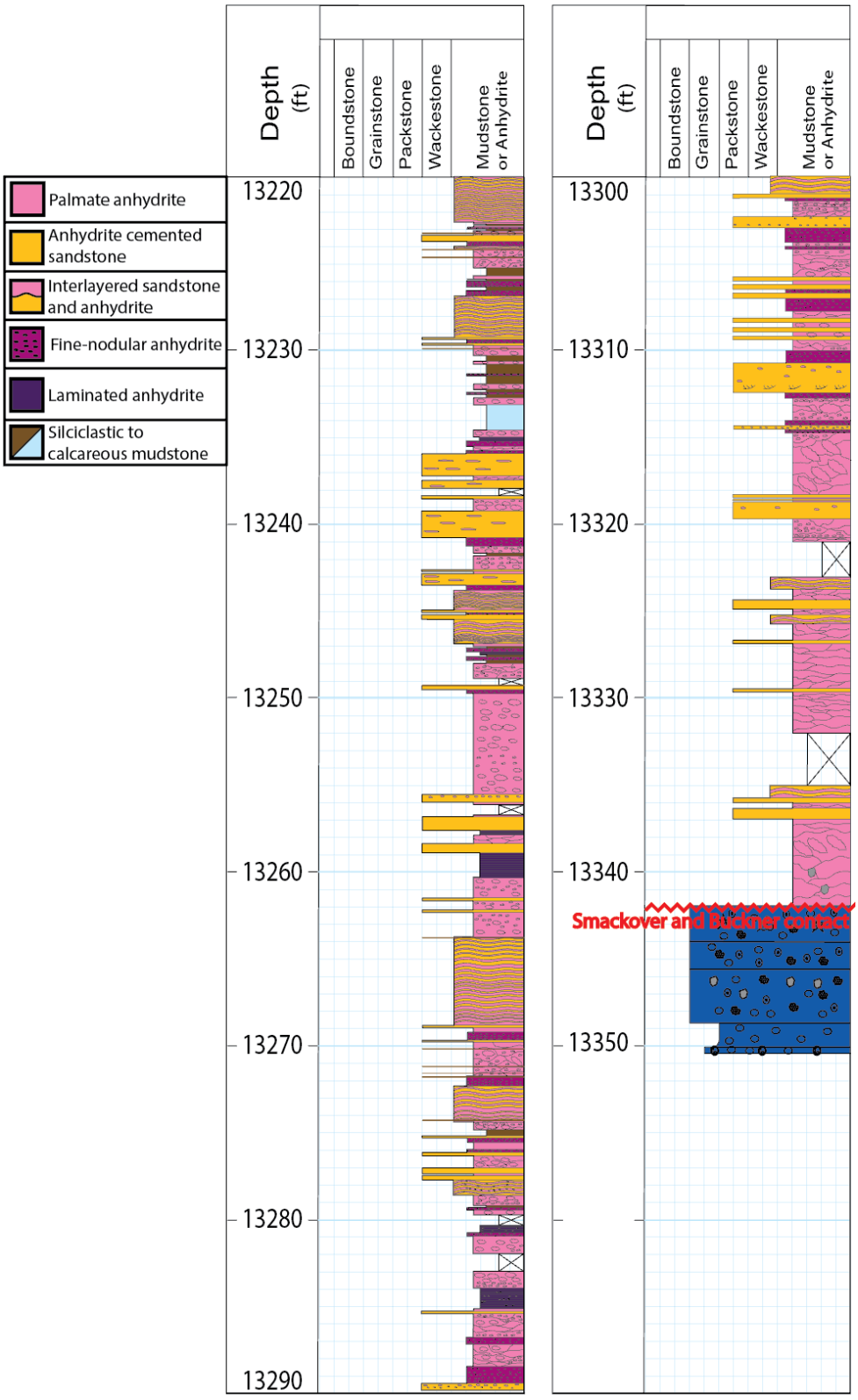
Palmate anhydrite
Anhydrite cemented sandstone
Interlayered sandstone and anhydrite
Fine-nodular anhydrite
Laminated anhydrite
Silciclastic to calcareous mudstone
Depth (ft)
Boundstone
Grainstone
Packstone
Wackestone
Mudstone or Anhydrite
13220
13230
13240
13250
13260
13270
13280
13290
Depth (ft)
Boundstone
Grainstone
Packstone
Wackestone
Mudstone or Anhydrite
13300
13310
13320
13330
13340
13350
Smackover and Buckner contact

Figure 12.

Figure 12: Vertical sequence of lithofacies within the Buckner Anhydrite section of the Travis Gas Unit No. 1 core. Refer to Figure 14 for the legend of features and lithofacies described in the section.

PALMATE ANHYDRITE

Description: The undisturbed to contorted palmate anhydrite contains variable amounts of dolomite, quartz silt, and clay minerals filling between the anhydrite. Palmate crystals are smeared, squeezed, and offset from one another when the anhydrite is distorted (Fig. 13C). Even the best-preserved palmate structures show signs of deformation, but their structure and size remain identifiable (Fig. 13B). Palmate structures range from 2 to 7 cm in height and they are elongated lobe-shaped features with multiple orientations that may radiate from a single point. In the lower portion of the Buckner section, the anhydrite is commonly deformed but further up section the anhydrite structures are better preserved. Intervals of palmate anhydrite are commonly separated or capped my mud drapes.

Interpretation: The formation of palmate structures is a clear indicator of subaqueous development. These palmate structures commonly grew into sub vertical bushels of palm-frond shaped crystals on the sediment surface in shallow, subaqueous hypersaline environments (salinas) (Schreiber et al., 1977; Schreiber et al., 1982; Loucks and Longman, 1987).

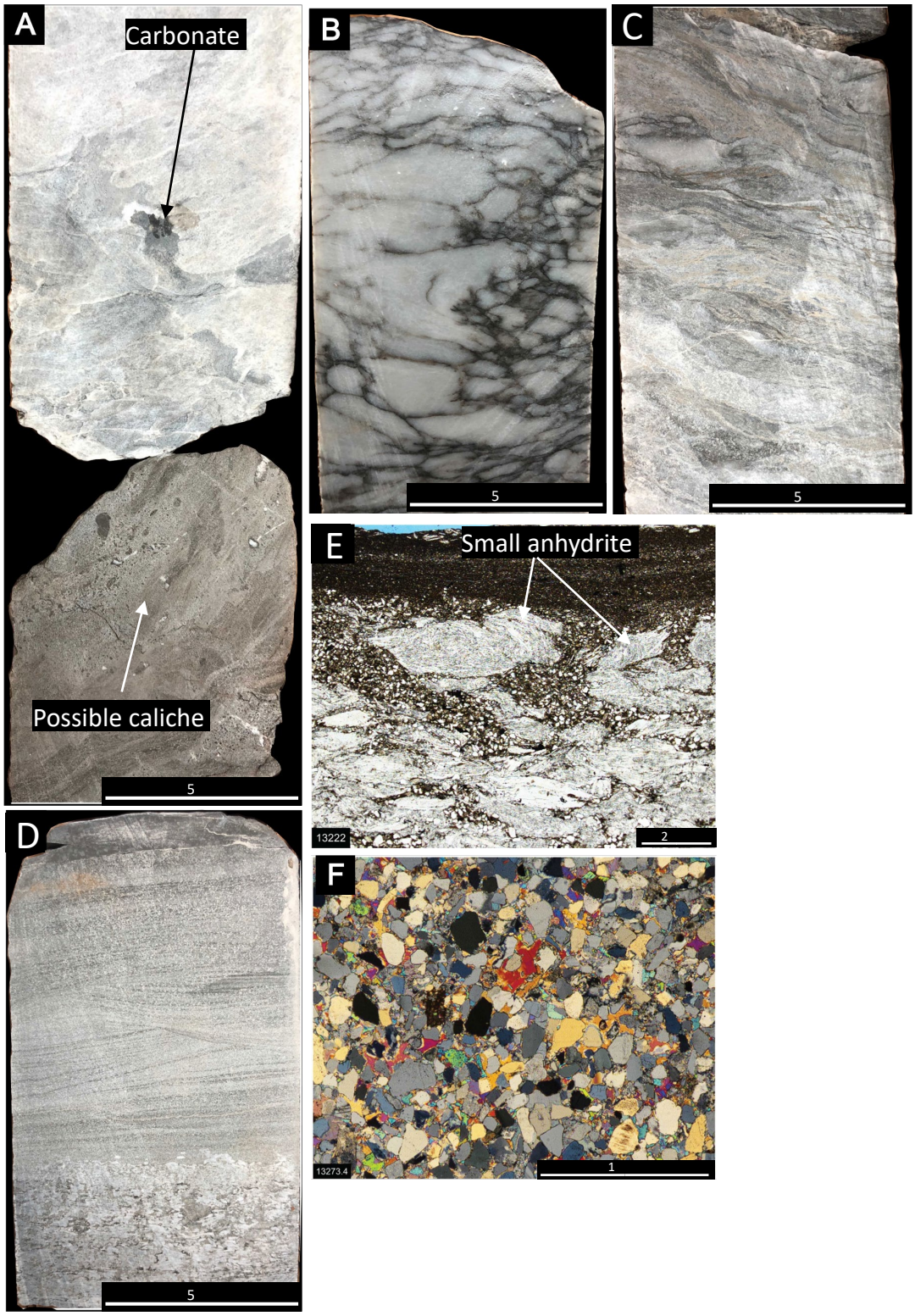
A
Carbonate
Possible caliche
5
B
5
C
5
D
5
E
Small anhydrite
13222
2
F
13273.4
1
Figure 13.

Figure 13: Buckner Anhydrite photographs. (A) General contact between the Smackover Formation and Buckner Anhydrite. The actual contact is missing. Smackover section appears to have potentially formed caliche crusts, gray clasts incorporated within the basal portion of the Buckner Anhydrite are carbonate and may be ripped-up Smackover clasts. (B) Highly distorted palmate crystals highlighted by dark seams. (C) Deformed anhydrite with streaks of quartz silt. (D) From the bottom up small rounded anhydrite, cross-bedded sandstones, planar laminations, and a clay seam. (E) Fining-upward sequence with small rounded anhydrite clasts within quartz silt fining up to laminated mudstone. (F) Anhydrite cemented quartz sandstone in cross-polarized light.

FINE-NODULAR ANHYDRITE

Description: This lithofacies is made up of thin-bedded moderately to well-sorted anhydrite nodules generally within a sandstone or mudstone matrix (Fig. 13C, E). The beds commonly occur at the base of the anhydrite cemented sandstone lithofacies and have fining-upward grading. In some sections, mostly near the lower portion of the interval, these nodules have been compressed and elongated.

Interpretation: The fine-anhydrite nodules are well sorted, rounded, and commonly concentrated at the base of sandstone packages. These nodules may have been eroded and transported as clasts in a subtidal setting. This is likely the case when the lithofacies is below the anhydrite cemented sandstone lithofacies. Additionally, these fine-nodules of anhydrite may indicate intervals of initial growth of palmate structures and/or nodules followed by burial preventing further growth.

ANHYDRITE CEMENTED SANDSTONE

Description: The quartz sandstones are well-sorted and are generally cemented with anhydrite (Fig. 13D, F). The sandstones are mostly massive, but occasionally ripples and cross beds are preserved (Fig. 13D). Sandstone packages are commonly capped by mud drapes and large displacive anhydrite nodules are observed within the upper portions of the sand packages.

Interpretation: The sandstone packages represent events of fluvial sedimentation that were probably the result of slightly wetter periods within the wadi environment. The fine-nodular anhydrite lithofacies commonly forms at the base of the sandstones and was likely the basal part of the flows depositing the sands.

Interlayered Sandstone and Anhydrite

Description: This lithofacies is composed of alternating sandstone and nodular anhydrite with sandstone proportions increasing vertically. The lithofacies lacks sedimentary structures.

Interpretation: This lithofacies may indicate periods of sustained subaerial exposure and more sabkha-like deposition with wadi/eolian influence. The anhydrite may have displacively formed within the sediment in response to variations in sediment-water saturation (Warren, 2006, p. 40). These anhydrite intervals were further buried by wadi or eolian sands and led to alternations of anhydrite and sand.

Siliciclastic to Calcareous Mudstone

Description: The siliciclastic mudstone lithofacies is composed of dark nonfossiliferous mudstone interbedded with anhydrite. In one section of the core there is a 2 ft thick interval of calcareous mudstone containing scarce peloids.

Interpretation: The siliciclastic mudstones suggest deposition from waning flows in fining-upward sequences and/or periods of low-energy suspension settling. These

mudstones may have been sourced by fluvial (wadi) input while the carbonate-rich mudstones were deposited when no siliciclastic source was available.

LAMINATED ANHYDRITE

Description: Laminated anhydrite intervals contain several types of deposits but are most characterized by the lamination of anhydrite. The types of beds include dolomite-rich anhydrites, clay drapes, medium-sized anhydrite nodules, small bedded anhydrite nodules, and some sandstones.

Interpretation: Laminated anhydrites generally form in subaqueous stagnant conditions typical of salina or salt-pan settings (Warren, 2006, p. 23).

CHAPTER 5: DISCUSSION

Depositional Model

The depositional model proposed by many authors for the Smackover along the gulf coast is that of a carbonate ramp (Ahr, 1973; Budd and Loucks, 1981; Ewing, 2001; Heydari and Baria, 2005). The lower Smackover is composed of the first marine sediments deposited in the East Texas basin during the early stages of platform development; therefore, ramp like depositional would be expected because no continental shelf had been established prior (Ahr, 1973; Ewing, 2001). Carbonate ramps are generally gently seaward dipping with facies belts controlled by energy related to fair-weather and storm-wave base but also by antecedent topography, storm deposits, sediment build ups, and tidal energy (Flugel, 2004, pg. 665). The actual depth of fair-weather and storm-wave base varies in relation to local hydrodynamic/climatic conditions and with time (Burchette and Wright, 1992). Below storm-wave base, lithofacies are controlled by paleotopography, salinity in stratified water columns, and oxygen levels. Homoclinal and distally steepened ramps are the two types of carbonate ramps. Homoclinal ramps have a continuous gradual slope into the basin and distally steepened ramps have an increase in slope in its distal portion (Flugel, 2004, pg. 665).

The Smackover-ramp depositional model proposed by this investigation is presented in Figure 15. Lithofacies present within the Travis GU No. 1 core are referenced to this model based on the original sediment characteristics and interpreted

associated physical and chemical processes. The ramp is subdivided into inner, middle, and outer ramp, which correspond to the upper Smackover, middle Smackover, and lower Smackover respectively. These ramp locations can be further subdivided into the distal outer ramp, proximal outer ramp, distal inner ramp, and proximal inner ramp. The following sections will discuss the Smackover lithofacies and their respective locations within the ramp model.

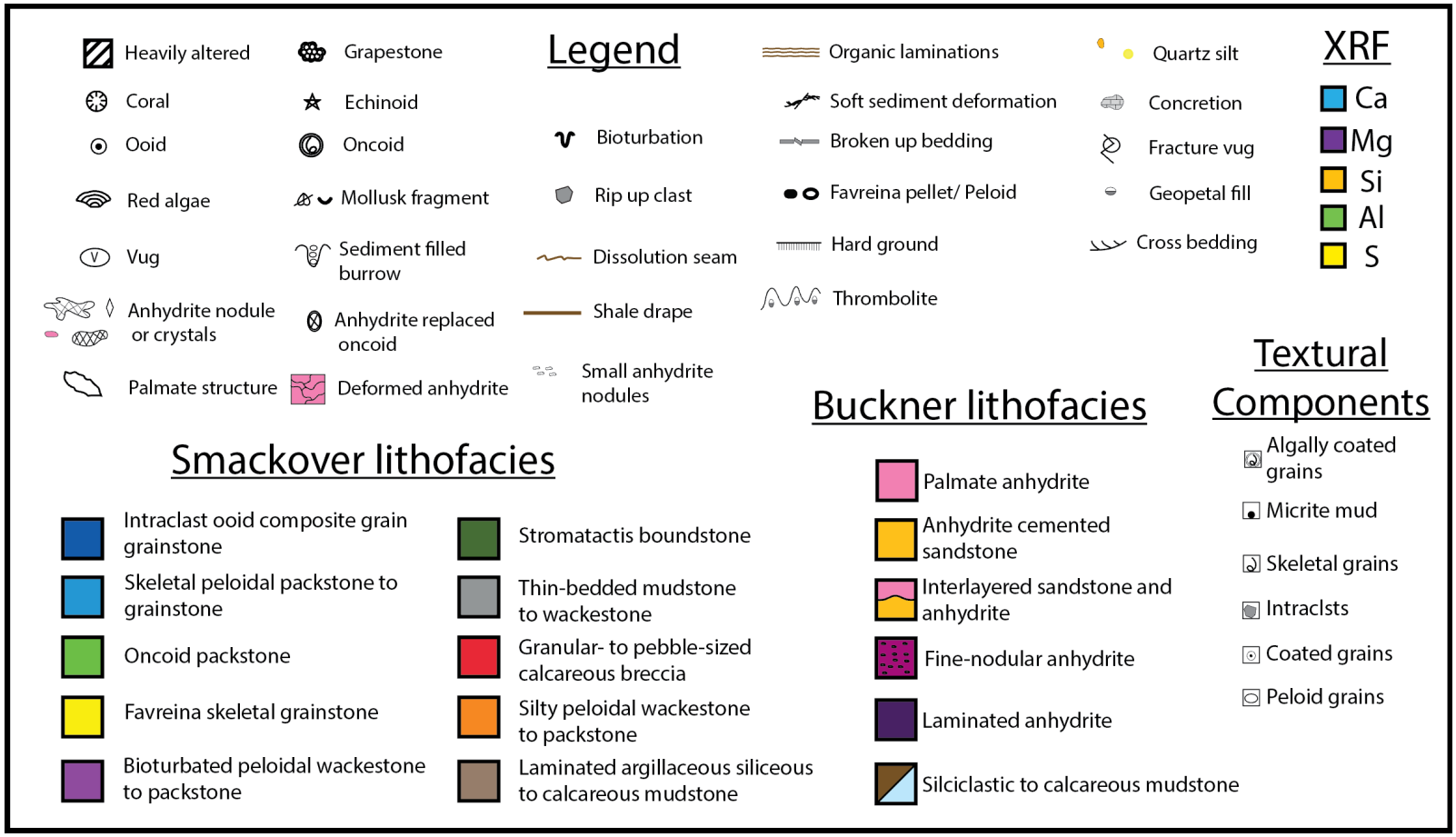
Legend
Heavily altered
Coral
Ooid
Red algae
Vug
Anhydrite nodule or crystals
Palmate structure
Grapestone
Echinoid
Oncoid
Mollusk fragment
Sediment filled burrow
Anhydrite replaced oncoid
Deformed anhydrite
Bioturbation
Rip up clast
Dissolution seam
Shale drape
Small anhydrite nodules
Organic laminations
Soft sediment deformation
Broken up bedding
Favreina pellet/ Peloid
Hard ground
Thrombolite
Quartz silt
Concretion
Fracture vug
Geopetal fill
Cross bedding
XRF
Ca
Mg
Si
Al
S
Smackover lithofacies
Intraclast ooid composite grain grainstone
Skeletal peloidal packstone to grainstone
Oncoid packstone
Favreina skeletal grainstone
Bioturbated peloidal wackestone to packstone
Stromatactis boundstone
Thin-bedded mudstone to wackestone
Granular- to pebble-sized calcareous breccia
Silty peloidal wackestone to packstone
Laminated argillaceous siliceous to calcareous mudstone
Buckner lithofacies
Palmate anhydrite
Anhydrite cemented sandstone
Interlayered sandstone and anhydrite
Fine-nodular anhydrite
Laminated anhydrite
Silciclastic to calcareous mudstone
Textural Components
Algally coated grains
Micrite mud
Skeletal grains
Intraclsts
Coated grains
Peloid grains

Figure 14.

Figure 14: Legend for lithofacies, biotas, textural elements, and XRF mineralogy for Figures 6, 12, and 15

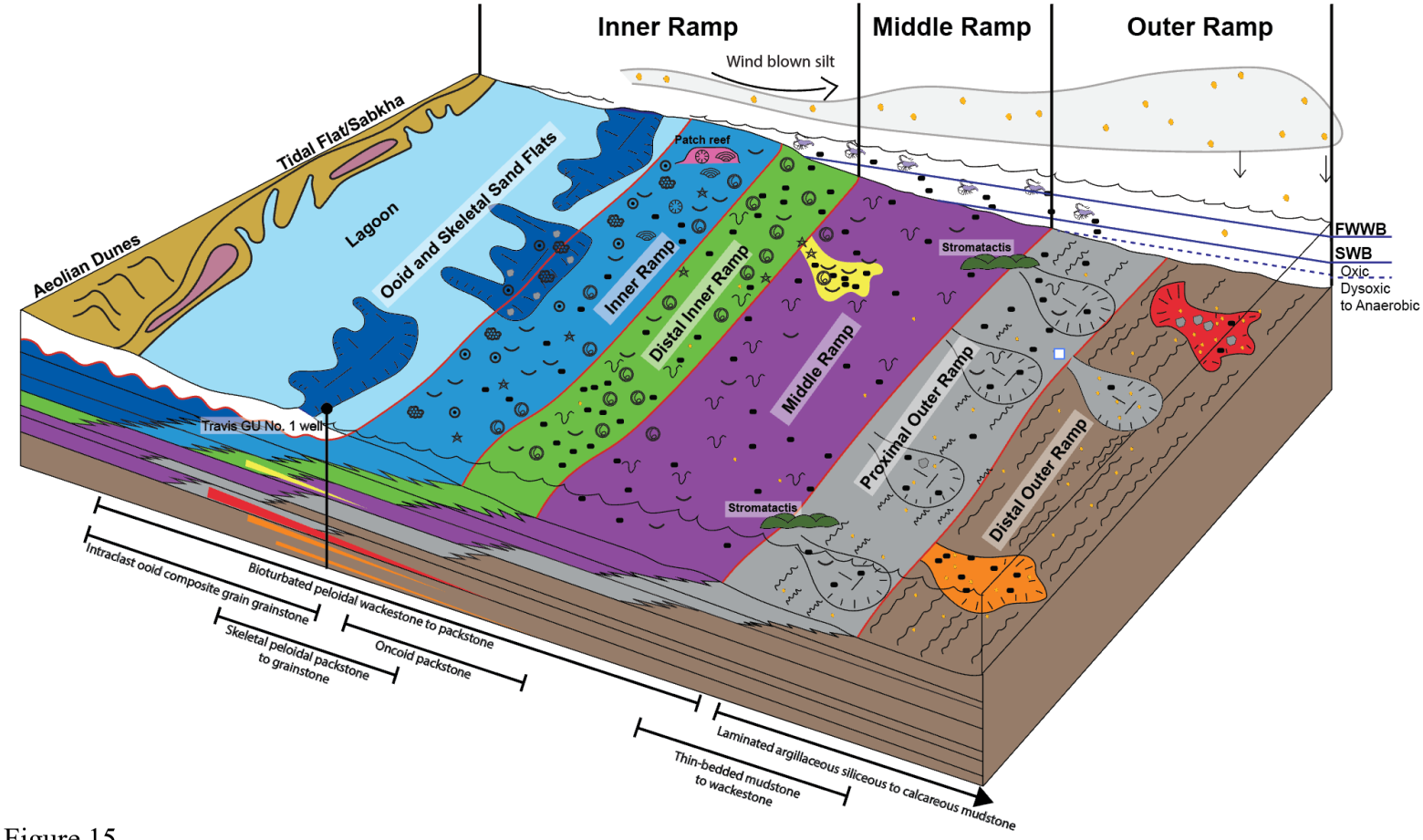
Inner Ramp
Middle Ramp
Outer Ramp
Wind blown silt
Tidal Flat/Sabkha
Aeolian Dunes
Lagoon
Ooid and Skeletal Sand Flats
Patch reef
Inner Ramp
Distal Inner Ramp
Middle Ramp
Proximal Outer Ramp
Distal Outer Ramp
Stromatactis
Stromatactis
FWWB
SWB
Oxic
Dysoxic
to Anaerobic
Travis GU No. 1 well
Intraclast ooid composite grain grainstone
Skeletal peloidal packstone
to grainstone
Bioturbated peloidal wackestone to packstone
Oncoid packstone
Thin-bedded mudstone
to wackestone
Laminated argillaceous siliceous to calcareous mudstone

Figure 15.

Figure 15: Depositional model of the East Texas Smackover section based on lithofacies identified in the Travis GU No. 1 core. The legend for this figure is presented in Figure 14.

LOWER SMACKOVER DEPOSITIONAL SYSTEMS AND FACIES TRACTS

The laminated mudstones of the lower Smackover were deposited on the distal portions of the carbonate ramp, at the base of the ramp or within the anoxic bottom waters. The climate during Smackover deposition was arid and set up evaporative environments that resulted in a landward increase in salinity (Heydari and Moore, 1994). Additionally, positive features such as the Angeline Caldwell Flexure (Fig. 1) may have restricted circulation of sea water between the East Texas basin and the Gulf of Mexico (Wood and Walper, 1974; Moore et al., 1988). These conditions could have led to elevated salinities within the East Texas basin and potentially produced a stratified water column. Super saturation of aragonite in sea water also explains the proliferation of ooid grainstones during the Late Jurassic (Moore et al., 1988; Heydari and Moore, 1994).

High salinities and low oxygen content within sea water restricts biodiversity in marine environments (Oschmann, 1993). This environmental stress may explain the presence of microbial features such as sulfur reducing microbial mats preserved in Smackover rocks. Microbial organisms are very resilient and thrive in stressed environments because these environments restrict metazoan grazers (Mancini et al., 2004; Schieber et al., 2007). Grazers inhibit microbial growth and quickly out compete microbial organisms for territory (Schieber et al., 2007). In the anoxic and elevated salinity environment that the lower Smackover sediments were deposited in, microbial

mats were able to develop periodically and are a dominant contributor of organic matter for the lower Smackover source rocks.

Within the laminated mudstones there are alternations between carbonate-rich laminae with quartz silt and organic-rich laminae. This alternation has many potential explanations. Heydari et al. (1997) suggested these variations were varves formed through suspension settling of organics supplied by algal blooms. They propose that these algal blooms were triggered by nutrients supplied by the ancestral Mississippi delta and nutrient levels related to climate variations. However, within the East Texas basin during the Oxfordian Stage, there is no mention in the literature of a drainage system to supply the nutrients that could induce the algal blooms. The lack of fluvial drainage along the East Texas basin is potentially caused by the Ouachita Mountain front shielding the basin from northwest-sourced weather systems. This resulted in moisture dumped on the northeast craton side of the mountains and hot Chinook winds spilling down the basin ward side, leading to arid conditions (Turner, 2001). Thus, two potential explanations are proposed for these alternations of laminae. The first is that organic-rich microbial mat growth is being interrupted by brief sedimentation events. These events may have been hemipelagic plumes or whitings that supplied carbonate muds to distal environments through suspension settling. Muds may have been partly supplied by coccolithophores, which were present during this time period. However, no coccolith material was observed in thin-section or scanning electron microscope analysis and these planktonic organisms have not been mentioned within Smackover literature. However, because of the high maturity level seen in the investigated core, they may have been obscured by diagenesis.

The second explanation is that the carbonate-rich laminae were formed through *in-situ* precipitation in microbial mat laminae. Given the correct water chemistry, syngenetic carbonate precipitation in microbial mats can take place (Thompson and Ferris, 1990; Pratt, 2001; Schieber et al., 2007). This may have been a response to changing bottom water chemistry towards more alkaline waters (Thompson and Ferris, 1990; Pratt, 2001).

The thin-bedded mudstones within the laminated mudstone lithofacies were probably deposited by dilute turbidity currents similar to the silty peloidal wackestone to packstone lithofacies. The flow deposits appear to be more mud-dominated in distal environments and as shallower-water Smackover lithofacies prograde into the basin, flow deposits became more peloidal and skeletal-rich. The core description in Figure 6 shows cycles, discernable by the bundling of mud-rich gravity flows, which may be controlled by potential fourth-order sea-level cycles. There appears to be a cycle top in the middle of the laminated lithofacies (13883 ft) and a second cycle at the top of the lithofacies (approx. 13820 ft) as it transitions to the silty peloidal wackestone to packstone lithofacies and is finally capped by the granular to pebble calcareous breccia lithofacies (debris flow). The presence of ripped up clasts of underlying lithofacies within the debris flow indicates some flows were erosive. These flows, early fracturing, and tilting of beds suggests the Smackover ramp was fairly active. This activity may have been trigged by early instability of the ramp as a result of the migration of underlying salt (Wilkinson, 1984).

Following the debris flow lithofacies there is a transition into thin-bedded mudstone to wackestone lithofacies, interpreted as stacked mud-rich gravity flow

deposits. The shift towards higher concentrations of flow deposits indicates increasing carbonate sediment being transporting down the ramp and suggests a more proximal depositional environment than the laminated mudstones and/or an increase in the amount of sediment being produced. In either case the increased sedimentation likely inhibited microbial mat growth. These thin-bedded mudstones are interbedded with the laminated mudstones, bioturbated mudstones, and buildups/boundstones (interpreted stromatactis boundstone lithofacies). The changes between lithofacies probably indicates variations in depth, sedimentation rate, and/or the position of the anoxic bottom water layer. These variations may all be linked and controlled by fourth-order sea level cycles. The thin-bedded mudstones are a transitional lithofacies between the lower ramp and the middle ramp. The mudstones display increasing skeletal content up section indicating an increase in the amount of sediments from shallower environments being transported in flows. Additionally, interbedding with bioturbated lithofacies becomes more common up section as well, suggesting a proximity to oxygenated waters. These observations point towards the lithofacies representing shallowing conditions or an increasing proximity to oxygenated waters.

The stromatactis boundstone lithofacies is relatively nondescript except for the distinct geopetal-filled voids and remnant growth structures. The matrix of the lithofacies is massively dolomitized such that the fine-scale matrix features are obliterated. Flugel (2004, p. 196) provides a variety of paleoenvironmental settings of stromatactis-rich rocks that he has summarized from the literature. In general, this lithofacies is associated with low-energy medium water depths ranging from above to below storm-wave base.

Additionally, they have been known to form at the flanks of sediment buildups like gravity flows in ramp environments (Flugel, 2004, p. 196). This environment interpretation agrees with the middle to outer ramp position proposed in the model.

MIDDLE SMACKOVER DEPOSITIONAL SYSTEMS AND FACIES TRACTS

The bioturbated peloidal wackestone to packstone is the most common lithofacies within the cored interval and is the primary lithofacies that comprises the middle Smackover (from approximately 13602 ft to13473 ft). Bioturbation obscures sedimentary features making it difficult to interpret depositional processes. Mud in this interval was probably transported into the environment by hemipelagic plumes, long-shore currents, or by gravity flows from shallower ramp environments (Burchette and Wright, 1992). Skeletal and algal coated grains such as those in the *Favreina* skeletal grainstone lithofacies were probably sourced from the up-dip shallower ramp related to storm-induced flows (Burchette and Wright, 1992). Biota in this oxygenated setting consumed organic matter leading to low TOC values. There is an increase in bioturbation, skeletal grains, and peloid types and sizes vertically in the section, suggesting increasingly favorable conditions for organisms. This may be related to an increasing supply of oxygen at the sediment water interface as the depositional environment became shallower. The bioturbated peloidal wackestone to packstone lithofacies could be interpreted as being deposited in a shallow-water lagoonal environment. However, because the lithofacies overlies strata deposited in distal environments and lacks grain-rich or shoal deposits it likely represents deposition in the middle ramp.

The middle ramp proposed in this model (Fig. 15) is defined by oxygenated bottom-water and sediment conditions and low-energy deposition. These conditions were likely present along a large portion of the Smackover ramp based on the abundance of the bioturbated peloidal wackestone to packstone lithofacies. The thickness and areal extent of the lithofacies is probably determined by the paleo position of storm-wave-base, anoxic bottom-water layer, and the slope of the ramp.

UPPER SMACKOVER DEPOSITIONAL SYSTEMS AND FACIES TRACTS

The upper Smackover lithofacies are heavily altered by diagenesis and fabric destructive dolomitization. However, as the lithofacies evolved from the oncoid packstone lithofacies through the skeletal peloidal packstone to grainstone lithofacies to the intraclast ooid/composite-grain grainstone lithofacies there is an overall upward decrease in carbonate mud, an increase in grainier lithofacies, and an increase in sorting suggesting shallower-water, higher-energy deposition. Additionally, the abundance of firm ground to fining-upward sequences through the three lithofacies indicate episodic depositional events of sedimentation that may be related to effects of large storms (Wanless et al., 1988).

The deposition of these lithofacies suggest wave energy was present, creating complex nearshore facies mosaics (Flugel, 2004, pg. 665). Adding to this complexity were topographic lows and highs formed by salt withdrawal and buildup in response to active salt movement taking place penecontemporaneously (Jackson, 1982; Wilkinson, 1984). Additionally, the presence of coral fragments and red algae within the grainstones

may indicate proximal patch-reef development. The oncoids packstone lithofacies is considered a transitional facies just below and within fair-weather-wave base, where bottom sediments were affected periodically by storm energy (Flugel, 2004, p. 136). Variations in the lithofacies indicate changes in the energy controlling bottom conditions and associated oncoid growth. The skeletal peloidal packstone to grainstone lithofacies were deposited in moderate- to high-energy waters above fair-weather-wave base. The occurrence of various skeletal grains such as red algae and coral fragments and various peloid types indicate a normal-marine. The intraclasts and ooid composite grain grainstone lithofacies is heavily dolomitized and is composed up of well-sorted intra-clasts and coated grains. It contains less skeletal organisms than the underlying lithofacies and may suggest elevated salinities in a more restricted interior setting. Lithofacies indicating a shoal complex are not clearly discernable within the investigated core. The intraclasts-ooid composite grain grainstone lithofacies may be a portion of a former shoal facies, but it has been eroded before the deposition of the overlying Buckner Anhydrite. The contact with the overlying Buckner Anydrite appears to be calichefied. The truncation of the upper Smackover and signs of exposure suggests the Buckner is in unconformable contact with the Smackover and there is strata eroded from the top of the Smackover section.

The dolomitization throughout the upper Smackover section are interpreted to have formed through evaporative reflux of dense Mg-rich brines supplied by the overlying Buckner Anhydrite (Dickinson 1969; Koepnick et al., 1985; Moore et al., 1988). The lithofacies affected by dolomitization may have had better hydrological

connectivity because these intervals were more porous and permeable. The fabric destroying dolomitization in the upper Smackover is probably obscuring lithofacies recognition that would allow a more complete interpretation of inner-ramp deposition.

Buckner Anhydrite Depositional Systems and Facies Tracts

The Buckner Anhydrite section of the core is challenging to interpret because of the distortion of features and the lack of common siliciclastic and carbonate depositional textures. However, the large amount of evaporites and development of palmate and laminated anhydrites indicates deposition in a subaqueous salina or salt pan like setting to probable sabkhas (Loucks and Longman, 1987). Additionally, the abundance of well-sorted, fine-grained sandstones indicates a proximal aeolian or wadi depositional process. The minimal amount of carbonate material in the section suggests either a proximity to terrestrial depositional environments or unfavorable water chemistry for carbonate precipitation. Also, the depositional setting may have been some distance from the open-marine carbonate factory. The anhydrite intervals represent subaqueous evaporite development while the sandy intervals are either episodic sediment depositional events or subaerial exposure. Exposure may have taken place as a result of minor sea-level changes or movement of underlying salt structures. During subaerial exposure, layers of anhydrites nodules probably developed at the high-saline water table, diagenetically emplacing nodules within the sand (Warren, 2006 p. 40). In the upper portion of the Buckner Anhydrite, mud drapes and mudstones become more common, indicating lower energy or more input of fine-grained sediment.

Additionally, the lack of carbonate material and abundance of quartz silt is significant. It is a stark contrast to the underlying Smackover section which is quartz-silt poor. This mineralogic contrast in addition to the calichified top of the upper Smackover supports the interpretation of an unconformable contact between the two members.

TOC and Source Rock Quality

The 28 total organic carbon (TOC) and Rock-Eval samples were taken from the Smackover section of the Travis GU No. 1 core. The results of the analysis are presented in Figures 16 to 18. Figure 16 shows the logged section with TOC values to the side of the core at the depths they were taken. Sample locations were selected targeting intervals with dark color, low carbonate content, and dissolution seams. The samples have very low hydrogen index (HI) values indicating elevated thermal maturities of organics. As a result of the low HI values, R_o and T_{max} values were unable to be calculated and kerogen type could not be identified using a pseudo-Van Krevlen plot. However, a regional study by Sassen (1990) identified oil generated by Type 1 kerogen from lower Smackover source rocks near the study area. The average TOC value is 0.48 wt% with the highest value being 1.59 wt%. The higher TOC values correspond to samples with low percent carbonate (Fig.17). In order to further evaluate the potential of the lower Smackover as a source rock a S1+S2 vs TOC plot was generated (Fig. 18). The plot shows that most points have poor source rock quality.

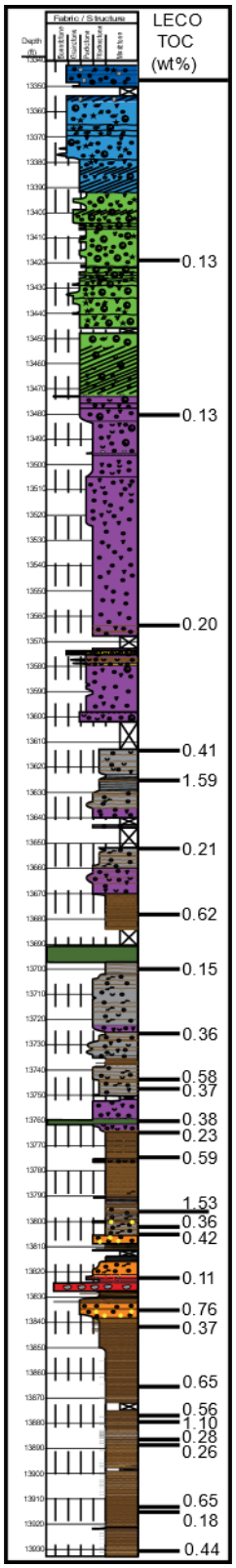

Figure 16: TOC values marked on core descriptions.

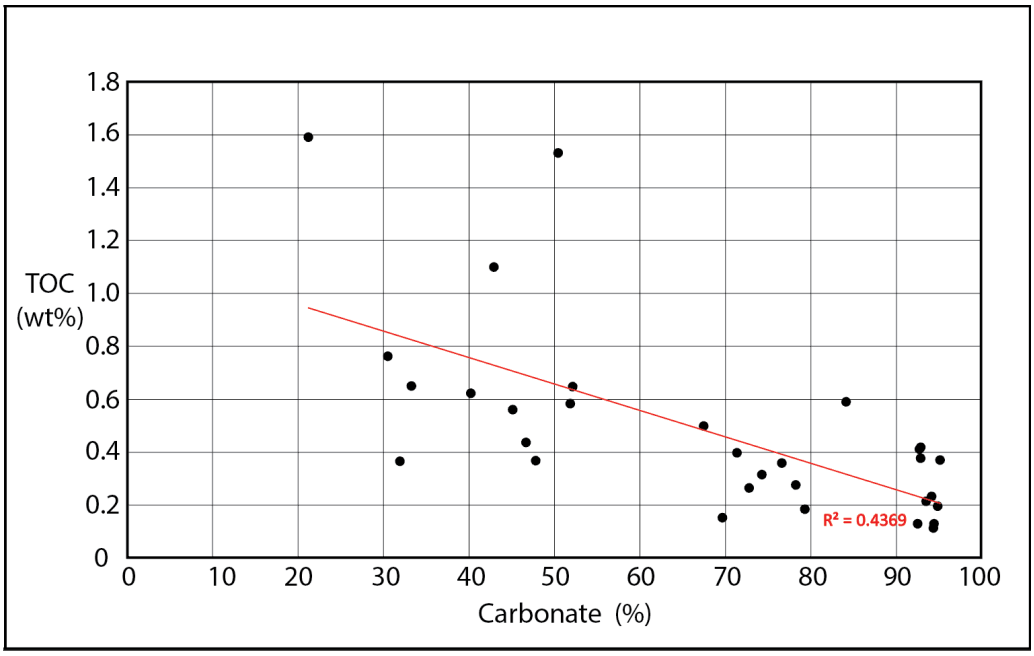

Figure 17: Percent carbonate versus TOC plot for Smackover samples. There is a fair inverse correlation between carbonate and TOC.

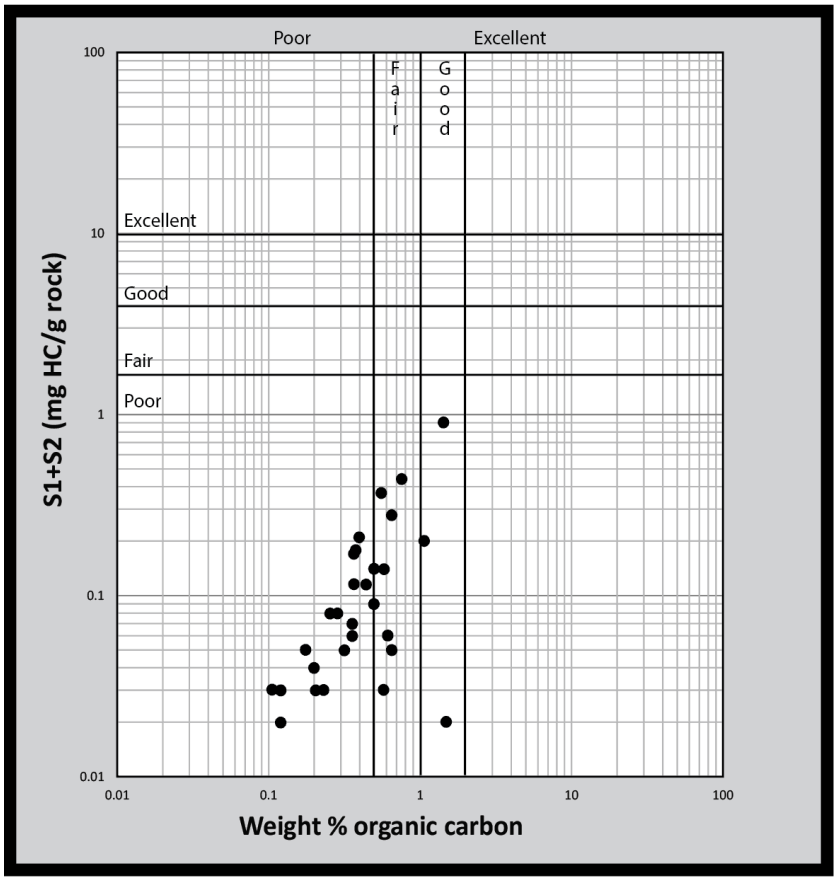

Figure 18: S1+S2 vs TOC plot for the Smackover samples.

Generation Potential	Wt% TOC, Siliciclastic mudrock	Wt% TOC, Carbonates
Poor	0.0-0.5	0.0-0.2
Fair	0.5-1.0	0.2-0.5
Good	1.0-2.0	0.5-1.0
Very Good	2.0-5.0	1.0-2.0
Excellent	>5.0	>2.0

Figure 19: Table providing guidelines for assessing the source-rock richness. From Law, (1999).

Understanding the apparent low source potential within this section is important for identifying localized source rock quality and/or unconventional reservoir potential of the lower Smackover. Assessing source rock potential for carbonate rocks is different than assessing the potential of siliciclastic rocks. There is a lower threshold for TOC values to indicate source rock in carbonates (Fig. 19) (Law, 1999). According to Sassen (1990) mean TOC for the entire Smackover including the non-source rock lithofacies is only about 0.5% and can reach TOC values as high as 10.3% along stylolites and dissolution seams. This is a result of non-carbonate material being concentrated into stylolites and dissolution seams during burial. However, the values obtained for the Smackover section in this study are low in comparison. This is probably caused by advanced levels of maturation, high expulsion efficiency, and potentially low original organic matter accumulation. High thermal maturities indicate degradation and expulsion of original organics but at least 50% of the organic matter is immobile and remains in the rock (personal communication Tongwei Zheng, Bureau of Economic Geology). This suggests that the original TOC of the rock was no more than double the measured TOC (personal communication Tongwei Zheng, Bureau of Economic Geology). Low concentrations of organic matter appear to be inversely related to carbonate sedimentation (Fig. 17). In the lower laminated mudstones, there is an inverse relationship between carbonate muds and organic matter with most of the organics concentrated along silt-rich laminae, dissolution seams, and stylolites. Because of this, lower Smackover mudstones with high concentrations of siliciclastic mud may be more

likely source rocks. Additionally, silt-rich laminae, stylolites, and dissolution seams are suggested to be lateral conduits for fluid migration (Sassen et al., 1987; Sassen, 1990). Furthermore, there are signs of early fracturing and instability within the lower mudstones potentially creating additional migration pathways. These conduits for flow and nearby faulting associated with underlying salt and basement structures may have led to early and efficient migration of hydrocarbons. Once migrated to overlying reservoirs the hydrocarbons experienced different levels of thermal maturation. Also, expulsed hydrocarbon lowers the S1 value obtained from Rock Eval analysis.

X-Ray Fluorescence (XRF)

Major- and trace-element XRF data was taken at 2-inch spacing along the length of the Smackover portion of the core. The major elemental data provide useful information for understanding variations in mineralogy along the section. Elemental abundances of Ca, Mg, Si, Al, Fe, and S are proxies of calcite, dolomite, and anhydrite (Ca), Dolomite (Mg), quartz and clay (Si), clay (Al), pyrite and sulfate minerals (S), and pyrite (Fe).

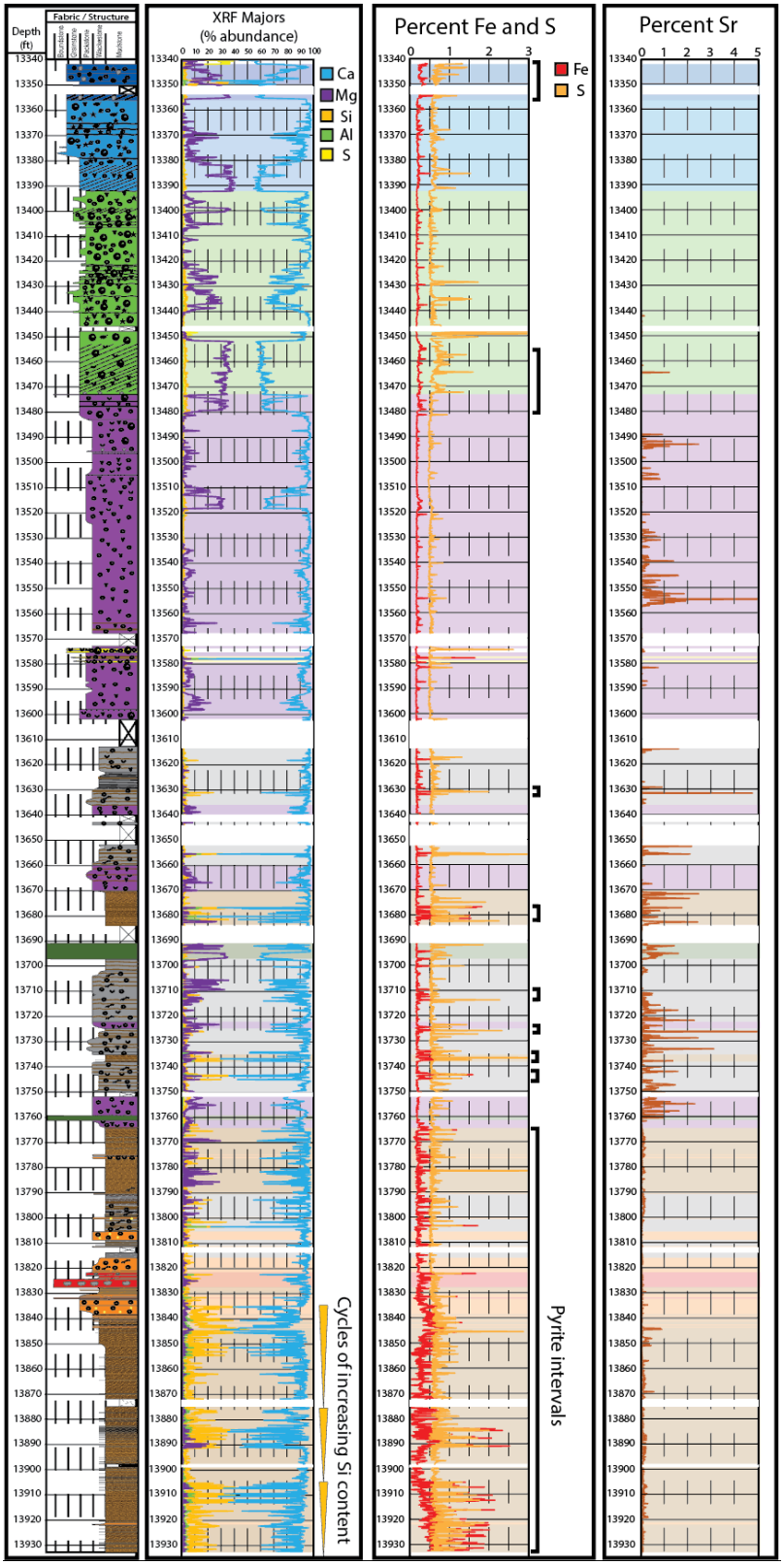
Depth (ft)
Fabric / Structure
Bioturbated
Laminated
Calcareous
Dolomitic
Mudstone
XRF Majors
(% abundance)
Ca
Mg
Si
Al
S
Percent Fe and S
Fe
S
Percent Sr
Cycles of increasing Si content
Pyrite intervals

Figure 20.

Figure 20: Major element curves (XRF data) versus depth in the Smackover section. Colored shading correlates to facies of the logged core.

TRENDS AND DISCUSSION

The most useful curves for understanding trends in the mineralogy of the Smackover section are Ca, Si, Mg, Al, S, Fe, and Sr. The curves that are presented in Figure 20 show trends in elemental abundances. As stated above the Si and Al curves can be used as a proxy for quartz-silt, feldspar, and clay minerals. The Si and Al curves show high values in the lower laminated mudstones and within dissolution seams throughout the core. In the lower laminated mudstone section, the Si curve shows multiple cycles of higher Si concentrations and a corresponding decrease in Ca. These cycles don't correlate with the cycles of massively bedded mudstones which suggests these may be unrelated trends. The cycles of increased Si might be connected to changes in the supply of windblown silt. These high Si values are helpful for identifying intervals with good expulsion efficiency and organic content due to the correlation between low carbonate and elevated TOC values observed in the source rock quality section of this study. Enhanced expulsion efficiency related to silt rich laminae and dissolution seams was originally proposed by Sassen et al. (1987).

The Mg and Ca curves inversely relate to one another with decreasing Ca concentrations corresponding to increasing Mg concentrations. This is a result of the formation of dolomite ($CaMg(CO_3)_2$) which replaces calcite ($CaCO_3$) and decreases the weight percent of Ca within the system in place of Mg. The presence of Mg within intervals of high Al may indicate the presence of Mg-rich clays such as illite or mixed-layer illite and smectite which have been identified in XRD measurements (Fig. 21).

Along the length of the core there are multiple intervals with some degree of dolomitization present. As mentioned earlier the dolomitization may be related to the reflux of Mg-rich brines from the Buckner Anhydrite above, but investigation into the source of dolomitization is beyond the scope of this study.

The S and Fe curves commonly correlate with one another along the length of the core, especially in the laminated mudstone intervals. This correlation is related to high concentrations of pyrite in intervals with organic matter. Within the laminated mudstones pyrite may have formed through primary deposition of pyrite framboids within sulfur reducing bacterial mats. Another interval where the S and Fe curves overlap is at the very top of the core in the dolomitized upper Smackover intervals. Here, large (50 to 300 microns) pyrite framboids have been identified in thin section (Fig. 8B, C). The two pyritized intervals are discussed in the pyrite section below. The Fe curve also shows a slight elevation in values within dolomitized intervals that are related to the presence of ferroan dolomites ($Ca(Mg, Fe)(CO_3)_2$) which were identified in XRD sampling (Fig. 21). Where the S curve does not correlate with the Fe curve it is indicating the presence of sulfate minerals (anhydrite and celestine) within the section.

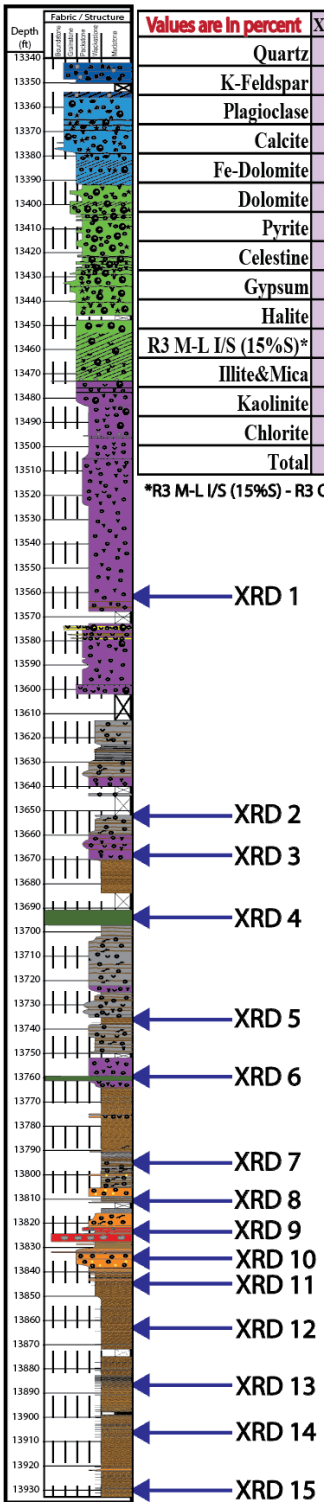

Values are in percent	XRD 1	XRD 2	XRD 3	XRD 4	XRD 5	XRD 6	XRD 7	XRD 8	XRD 9	XRD 10	XRD 11	XRD 12	XRD 13	XRD 14	XRD 15
Quartz	0.9	2.1	1.9	0.7	6.7	2.3	16.1	34.4	1.9	42.8	25.2	39.3	16.7	38.3	26.1
K-Feldspar	0	0	0	0	0	0	1.8	6.8	0	6.3	4.2	5.7	2.5	6.3	6.9
Plagioclase	0	0	0	0	0	0	1.8	5.1	0	5.6	3.1	5.2	2.5	7	2.3
Calcite	90.5	93.4	70	1.6	11.1	57.6	7.5	14.5	90.6	19.2	19.1	9.4	48.8	9.9	25
Fe-Dolomite	0	0	0	0	29.5	0	0	0	3.8	0	0	0	20.8	0	0
Dolomite	2.9	1.3	24.8	90.7	0	33.8	65.1	14.1	0	7.7	25.7	23.6	0	21.4	19.3
Pyrite	0.7	0	0	0	0	0	1.3	4.1	0.4	3.2	10	2.7	2.3	2.8	3.3
Celestine	0	0	0	3.7	44.7	0	0	0	0	0	0	0	0	0	0
Gypsum	0	0	0	0	0	0	0.4	1.1	0	1.4	3.4	1.2	0.8	2.3	2
Halite	0	0	0	0	0	2	0	0	0	0.4	0	0.4	0.3	0.7	1.9
R3 M-L I/S (15%S)*	0	0	0	0	0	0	0	1.1	0	0.7	1	1.1	1.2	1.4	1.3
Illite&Mica	5	3.2	3.3	3.3	8	4.3	6	18.8	3.3	12.7	8.3	11.4	4.1	9.9	10
Kaolinite	0	0	0	0	0	0	0	0	0	0	0	0	0	0	0.8
Chlorite	0	0	0	0	0	0	0	0	0	0	0	0	0	0	1.1
Total	100	100	100	100	100	100	100	100	100	100	100	100	100	100	100

*R3 M-L I/S (15%S) - R3 Ordered Mixed-Layer Illite/Smectite with 15% Smectite Layers

Figure 21.

Figure 21: XRD sample locations plotted against core description. Fifteen XRD analyses are present in the table and columns are shaded based on the sampled lithofacies.

XRF analysis is able to detect Sr as a trace element (ppm levels). However, within the Smackover section, percent levels were detected. In thin section, celestine crystals ($SrSO_4$) were identified filling in geopetal vugs and burrows as well as forming displacive crystals in thick dissolution seams. The presence of the celestine was also confirmed by XRD analysis (Fig. 21). High Sr values are detected in two main intervals of the core; the upper part of the lower Smackover and the upper portion of the middle Smackover. Elevated Sr concentrations in carbonate rocks are typically associated with original aragonite mineralogy (Kinsman, 1969). This is a result of the high Sr concentrations of aragonite as Sr more readily replaces Ca anions in aragonite compared to calcite (Kinsman, 1969). These high Sr intervals may represent different trends depending on whether the pore systems were open or closed. In a closed system the Sr concentration of the dissolved aragonite grains will equal the Sr concentration of the re precipitated carbonate minerals (Kinsman, 1969). In an open system grains are dissolved, and Sr is concentrated into a diagenetic brine that migrates out of the system (Kinsman, 1969). The diagenetic brines eventually precipitate Sr-rich minerals along permeable pathways as they migrate through the subsurface. In the closed system scenario, the Sr-rich intervals detected in the section may indicate trends related to the original chemistry of the carbonate muds forming the rocks. In the open system scenario, the Sr-rich intervals could have been pathways for diagenetic brines during early burial. Regardless of the scenario taking place, the intervals with high Sr values may suggest periods of aragonite deposition. Also, Sr could have been sourced by evaporite deposition.

However, if this were the case then high Sr would be expected to be more common in the upper Smackover section. This is significant because the Jurassic was a time of calcium carbonate precipitation from seawater (Sandberg, 1983). Heydari and Moore (1994) observed variations in ooid mineralogy from aragonite to calcite in Smackover shoals in the Mississippi salt basin. They proposed that this variation in mineralogy was related to a salinity gradient established within the basin during arid climatic conditions. The intervals with high Sr values for this study may also represent a similar process taking place during deposition within the East Texas basin.

Isotope Data

RESULTS

The $\delta^{13}C_{carb,}$ $\delta^{18}O_{carb}$, and $\delta^{13}C_{org}$ curves for the Smackover section of the core are presented alongside the core description in Figure 22. The main curve represents a 5-point moving average of the data. The data points in red represent intervals with high concentrations of Mg and thus are heavily dolomitized. The $\delta^{13}C_{org}$ measurements were taken after acidification of carbonate material; however, because of the high concentration of dolomite in some samples it was difficult to dissolve all of the carbonate material. Residual carbonate material produces unreliable results, so these data pointes were deleted from of the dataset resulting in a total of 244 organic carbon data points.

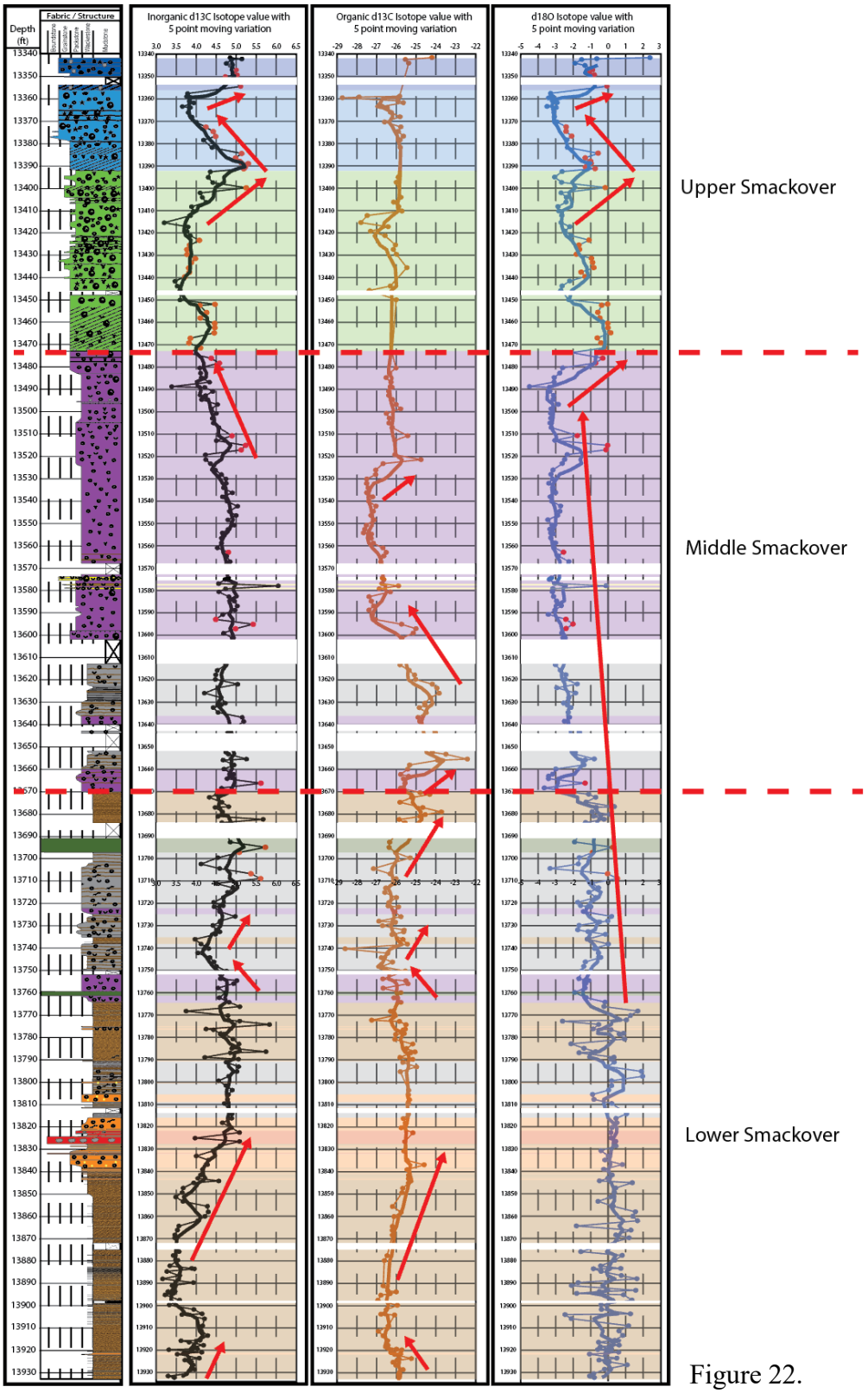
Depth (ft)
Fabric / Structure
Inorganic d13C Isotope value with 5 point moving variation
Organic d13C Isotope value with 5 point moving variation
d18O Isotope value with 5 point moving variation
Upper Smackover
Middle Smackover
Lower Smackover

Figure 22.

Figure 22: The $\delta^{13}C_{carb}$ (black), $\delta^{18}O_{carb}$ (blue), and $\delta^{13}C_{org}$ (brown) curves are presented alongside the logged Smackover section. The thick curve is a 5-point moving average of the data points. Red data points have very high concentrations of Mg indicating dolomitization. The shading color corresponds to the facies in the logged section and arrows highlight major trends.

Following an interval at the base of the core with increasing $\delta^{13}C_{carb}$ values (Δ~0.9‰, ~3.2 ‰ to 4.1 ‰) and decreasing $\delta^{13}C_{org}$ values (Δ ~0.5‰, ~-26 ‰ to -26.5‰), the $\delta^{13}C_{carb}$ and $\delta^{13}C_{org}$ curves show signs of covariation along the Smackover interval. The curves gradually increase towards heavier values ($\delta^{13}C_{carb}$: Δ ~1.8 ‰, ~3.2‰ to~5‰ $\delta^{13}C_{org}$: Δ ~1‰, ~-26.5 ‰ to -25.5 ‰) up through the lower Smackover. These heavier $\delta^{13}C_{carb}$ and $\delta^{13}C_{org}$ values are sustained with a brief decrease and increases in values ($\delta^{13}C_{carb}$: Δ~1‰ $\delta^{13}C_{org}$: Δ ~1.5‰) (13760 ft to 13720 ft) . Following the decrease, the two curves de couple with the $\delta^{13}C_{org}$ increasing sharply towards heavy values (Δ ~2.5‰, ~-26‰ to -23.5‰) at the boundary between the lower and middle Smackover. This trend in $\delta^{13}C_{org}$ values is followed by a gradual decline towards lighter values (Δ ~3.5‰, ~-23.5‰ to -27‰) into the middle Smackover. As the $\delta^{13}C_{org}$ curve fluctuates, the $\delta^{13}C_{carb}$ curve remains constant (between ~4.5‰ and ~5‰), with some 0.5 ‰ oscillations, until it gradually decreases towards lighter values (Δ ~1.5‰, 5‰ to 3.5‰) at the transition from the middle to upper Smackover. As the $\delta^{13}C_{carb}$ starts to decrease into the upper Smackover the $\delta^{13}C_{org}$ values sharply increase (Δ ~1.5‰, ~-27.5‰ to -26‰) and remain constant into the upper Smackover. The $\delta^{13}C_{carb}$ values show a small increase towards heavier values (Δ ~1.5‰) with a reciprocal fall back down to the previous level (3.7‰) in the middle of the upper Smackover. At the top of the section near the contact between the Buckner Anhydrite there is a sharp and sustained increase towards heavier $\delta^{13}C_{carb}$ values (Δ ~1.2‰). The $\delta^{18}O_{carb}$ curve shows a high degree of variability ($\pm$2‰) within the lower Smackover, in the laminated or thin bedded mudstone

lithofacies but averages ~0‰. Following the thin bedded mudstone facies, the $\delta^{18}O_{carb}$ consistently and gradually decrease (Δ ~3‰, ~0‰ to -3‰) to the boundary between the middle and upper Smackover. Within the upper Smackover section, the $\delta^{18}O_{carb}$ experiences multiple shifts towards heavier values (Δ ~2‰ to Δ ~3‰) corresponding with the dolomitized intervals and covaries with the $\delta^{13}C_{carb}$ for the last two shifts.

BULK ISOTOPE DATA AND DIAGENETIC INFLUENCES

Bulk sediment samples were collected because they best characterize the average inorganic carbon values for marine systems in pelagic sediments (Shackleton, 1987). The Smackover interval is mostly composed of micrite, aside from the upper grainstone portion, making it reliable for relating $\delta^{13}C_{carb}$ to seawater signals (e.g., Immenhauser et al.,2003; Föllmi et al., 2006; Louis-Schmid et al., 2007).

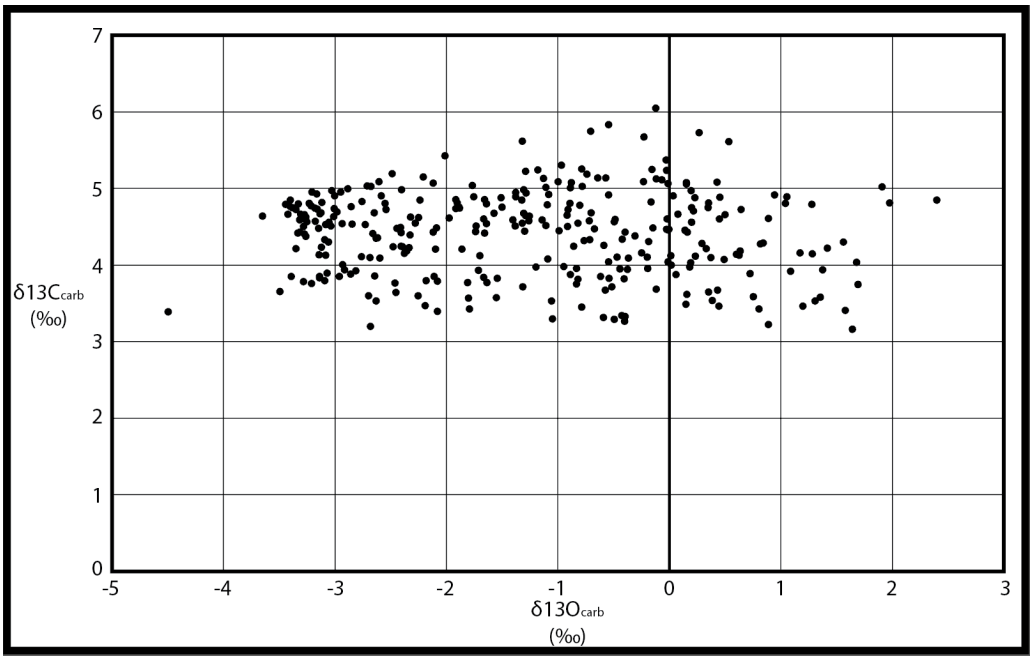

Figure 23: Cross plot of $\delta^{18}O_{carb}$ versus $\delta^{13}C_{carb}$ values. Shows little correlation, if any, suggesting negligible meteoric diagenesis.

To utilize the isotopic data as an interpretive tool for primary deposition and/or global isotopic signatures the effects of secondary alteration must be ruled out. These effects include meteoric diagenesis, burial diagenesis, and dolomitization. Meteoric diagenesis was likely negligible because the Smackover is a subsurface formation and was deposited in a marine environment with little exposure to freshwater fluids aside from the potential calichification at the Smackover-Buckner contact. The effects on the isotope curves are generally identified by looking for covariation of $\delta^{18}O_{carb}$ and $\delta^{13}C_{carb}$ values (Allen and Matthews, 1982). The curves show very little covariation other than the two excursions towards positive values at the top of the section (Fig. 22). Additionally, a cross plot of $\delta^{18}O_{carb}$ and $\delta^{13}C_{carb}$ values (Fig. 23) shows very low correlation between the two datasets suggesting the influence of meteoric diagenesis is negligible (Allen and Matthews, 1982). As a result of the abundant pelagic carbonate muds in the Smackover section, water-rock interactions and late cements are limited, so, burial diagenesis is also likely negligible (Edwards et al., 2015; Eltom et al., 2018). The formation of dissolution seams involved the dissolution and reprecipitation of calcite grains but likely occurred during shallow burial minimizing the effects on isotopic values. The upper Smackover dolomitized intervals are thought to be formed through reflux dolomitization of Mg-rich brines (Budd and Loucks, 1981; Harwood and Fontana, 1983; Hancharik, 1984; Stewart, 1984; Koepnick et al., 1985; Moore et al., 1988). The alteration of calcium carbonate to dolomite causes a 3-4‰ shift towards heavier oxygen isotope values and has a small or negligible effect on inorganic carbon values (Land, 1980). This shift is observed in the

$\delta^{18}O_{carb}$ data resulting in values that do not reflect depositional conditions over dolomitized intervals. The effect of dolomitization on the $\delta^{13}C_{carb}$ curve is questionable owing to the positive shifts in values covarying with $\delta^{18}O_{carb}$ values within upper Smackover dolomitized intervals. The $\delta^{13}C_{org}$ data is not affected by diagenetic processes but may be influenced by migrated bitumen. Within the dolomitized and grain-rich intervals of the upper Smackover, migrated hydrocarbons are observed filling pore spaces in thin section as bitumen. This migrated organic matter does not represent primary depositional $\delta^{13}C_{org}$ values thus making them unreliable for interpretation where present. Anomalous values in any of the three curves may be a result of sampling dissolution seams or fractures which may have been pathways for late diagenetic fluids potentially altering isotopic values. There is an increase in the variability of isotope values, especially in the $\delta^{18}O_{carb}$ data, within the laminated mudstone and to a lesser extent within the thin-bedded mudstone interval. However, within the bioturbated packstones there is low variability with samples providing a clear trend. The variations in $\delta^{18}O_{carb}$ isotope values within the laminated mudstone lithofacies may be a result of salinity and/or temperature gradients up the paleo ramp or stratification of the water column. Muds were sourced from environments further up the paleo carbonate ramp and transported into deeper settings by hemipelagic plumes and gravity flows. The positions along the ramp in which the muds were formed may have had varying salinities and temperatures causing muds to form with a range of isotopic concentrations.

INTERPRETATION AND CORRELATION OF ISOTOPE TRENDS

The global isotope curve for the Oxfordian constructed predominantly by studies in Europe (O'Dogherty et al., 2018 and references therein) and, more recently, in Saudi Arabia (Eltom et al., 2018; Al-mojel et al., 2018). These studies focus on the western and northwestern regions of the paleo Tethys (Fig. 24). The paleo GOM was situated within a restricted seaway between the Tethys and Panthalassia making this curve valuable for global studies, particularly because many authors have postulated that this seaway opened circulation between the two oceans during the late Oxfordian (O'Dogherty et al., 2018 and references therein). The previous studies have identified a ~1.5 to ~2 ‰ positive shift towards heavier $\delta^{13}C_{carb}$ values during the middle Oxfordian and a gradual decrease towards lighter $\delta^{13}C_{carb}$ values in the upper Oxfordian towards the Kimmeridgian boundary. There is a debate in the literature regarding the cause for the global $\delta^{13}C_{carb}$ isotope shifts. However, to discuss the global cause of these shifts is outside the scope of this study. This study focuses on whether the Smackover curve is corelative to global curves. The resolution and quality of published curves over the Oxfordian interval vary, making it difficult to do detailed correlation. Most published curves contain biozone age-control along with isotope curves to facilitate correlation. However, for this section of the Smackover in northeast Texas there is no such control. Despite this, $\delta^{13}C_{carb}$ trends are similar to published curves showing a 1.5 ‰ increase in $\delta^{13}C_{carb}$ and $\delta^{13}C_{org}$ in the lower Smackover followed by a gradual decrease towards lighter values in the upper Smackover (Fig. 25). The values for the $\delta^{13}C_{carb}$ for the Smackover section are on average 1.5-2 ‰ higher than other publish curves and it appears to be a bulk shift in values. This

shift may be related to local conditions of the East Texas basin. These conditions may be associated with a lack of drainage into the basin, as previously discussed, causing less light carbon from terrestrial organics to be introduced into the system (Saltzman and Thomas, 2012). Additionally, it could be a sign of an overall increase in organic matter deposition and preservation causing light carbon to be sequestered in organic matter, driving $\delta^{13}C_{carb}$ towards heavier values (Saltzman and Thomas, 2012). High resolution curves from Eltom et al., 2018 and references therein show detailed datasets along the Oxfordian interval and correlate well with the Smackover section (Fig. 25). The southern Tethys curves show a 1.5 ‰ increase followed by a decrease in values and another increase. Following the middle Oxfordian increase there is a decrease in the upper Oxfordian and multiple small positive excursions leading into the Kimmeridgian boundary. This correlation falls within the generally understood timeframe of Smackover deposition (lower Oxfordian boundary to the Kimmeridgian boundary) and suggests these curves may be globally correlated. The European curves correlate with the Smackover section over broad trends, but detailed correlation is challenging. This may be because of low-resolution, sampling of platform carbonates (Al-mojel et al., 2018), or variability related paleo latitude.

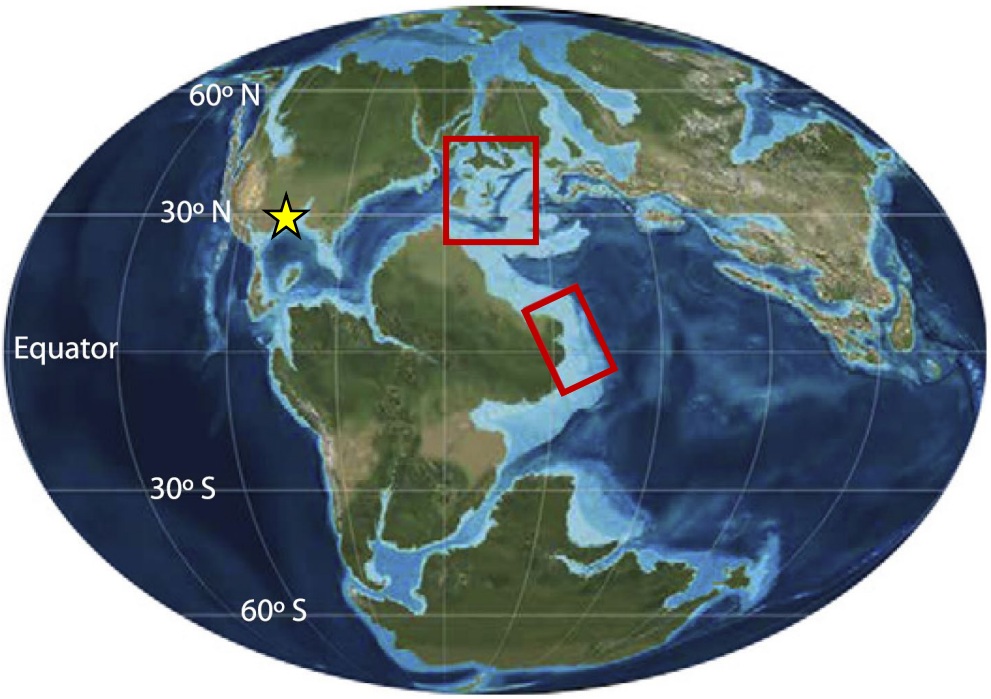

Figure 24: Paleogeographic map of the Tethys Ocean. the red boxes are the areas focused on in previous studies. The star is the location of this study. Base map courtesy of Ron Blakey (http://jan.ucc.nau.edu/~rcb7/).

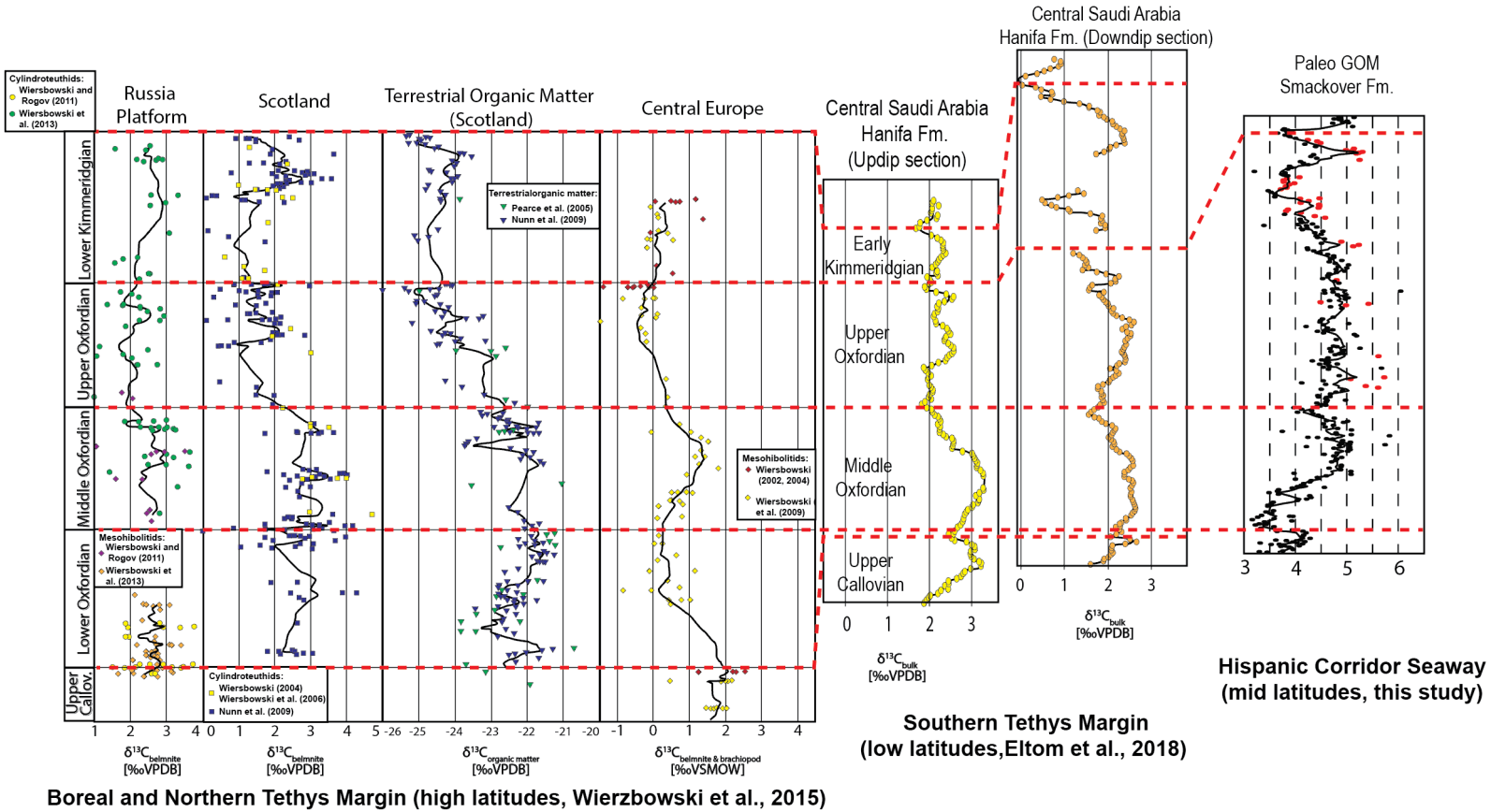
Cylindroteuthids:
Wiersbowski and Rogov (2011)
Wiersbowski et al. (2013)
Russia Platform
Scotland
Terrestrial Organic Matter (Scotland)
Central Europe
Central Saudi Arabia Hanifa Fm. (Updip section)
Central Saudi Arabia Hanifa Fm. (Downdip section)
Paleo GOM Smackover Fm.
Lower Kimmeridgian
Upper Oxfordian
Middle Oxfordian
Lower Oxfordian
Upper Callov.
Terrestrialorganic matter:
Pearce et al. (2005)
Nunn et al. (2009)
Mesohibolitids:
Wiersbowski (2002, 2004)
Wiersbowski et al. (2009)
Mesohibolitids:
Wiersbowski and Rogov (2011)
Wiersbowski et al. (2013)
Cylindroteuthids:
Wiersbowski (2004)
Wiersbowski et al. (2006)
Nunn et al. (2009)
Early Kimmeridgian
Upper Oxfordian
Middle Oxfordian
Upper Callovian
δ13Cbelmnite [‰VPDB]
δ13Cbelmnite [‰VPDB]
δ13Corganic matter [‰VPDB]
δ13Cbelmnite & brachiopod [‰VSMOW]
δ13Cbulk [‰VPDB]
δ13Cbulk [‰VPDB]
Boreal and Northern Tethys Margin (high latitudes, Wierzbowski et al., 2015)
Southern Tethys Margin (low latitudes,Eltom et al., 2018)
Hispanic Corridor Seaway (mid latitudes, this study)

Figure 25.

Figure 25: Comparison between δ13C records of central Saudi Arabia, the Boreal and northern Tethys Oceans and the Paleo GOM. Data from Wierzbowski et al. (2006, 2009, 2013, 2015), Nunn and Price (2010), and Eltom et al., 2018. Figure modified from Eltom et al., 2018.

When $\delta^{13}C_{org}$ and $\delta^{13}C_{carb}$ curves covary, they likely reflect a global signal because the values of each are inversely linked owing to the sequestration of lighter carbon by organics (Saltzman and Thomas, 2012). When the $\delta^{13}C_{org}$ and $\delta^{13}C_{carb}$ are out of covariation it likely represents a local change in the carbon isotope ratios. Within the $\delta^{13}C_{org}$ curve there are two such intervals, one at the base of the Smackover section where there is an increase in $\delta^{13}C_{carb}$ and corresponding decrease in $\delta^{13}C_{org}$ and another in the middle Smackover where there are variations in $\delta^{13}C_{org}$ with no shared signal in the $\delta^{13}C_{carb}$ curve (13710 ft to 13590 ft). The trend at the base of the section may reflect a local increase in organic productivity and a reciprocal depletion in light carbon pushing the $\delta^{13}C_{carb}$ towards heavier values (Saltzman and Thomas, 2012). The trend within the middle Smackover takes place at the transition from oxygen restricted to oxygenated waters. Excursions in $\delta^{13}C_{org}$ may reflect changes in the way organic matter is produced by organisms and/or how organic matter is reprocessed by organisms that ingest organics at the sediment water interface (Jenkyns et al., 2002).

$\delta^{18}O_{carb}$ values are commonly considered unreliable and inaccurate when acquired through bulk isotopic analysis (Weissert and Erba, 2004). Within the Smackover section the $\delta^{18}O_{carb}$ curve contains high-amplitude variability and shifts in values related to dolomitization suggesting the curve may not be reliable for interpretation. However, there is a clear trend towards lighter $\delta^{18}O_{carb}$ values through the section, which is consistent with trends identified in multiple studies of belemnites and oysters in northern Europe (Jenkyns et al., 2002 and references therein). The studies show an excursion towards high

$\delta^{18}O_{carb}$ values at the Callovian-Oxfordian boundary and then a decline from the boundary into Kimmeridgian time. This is consistent with the decline observed within the Smackover section and may support their interpretation of this trend being globally reproducible (Fig. 26).

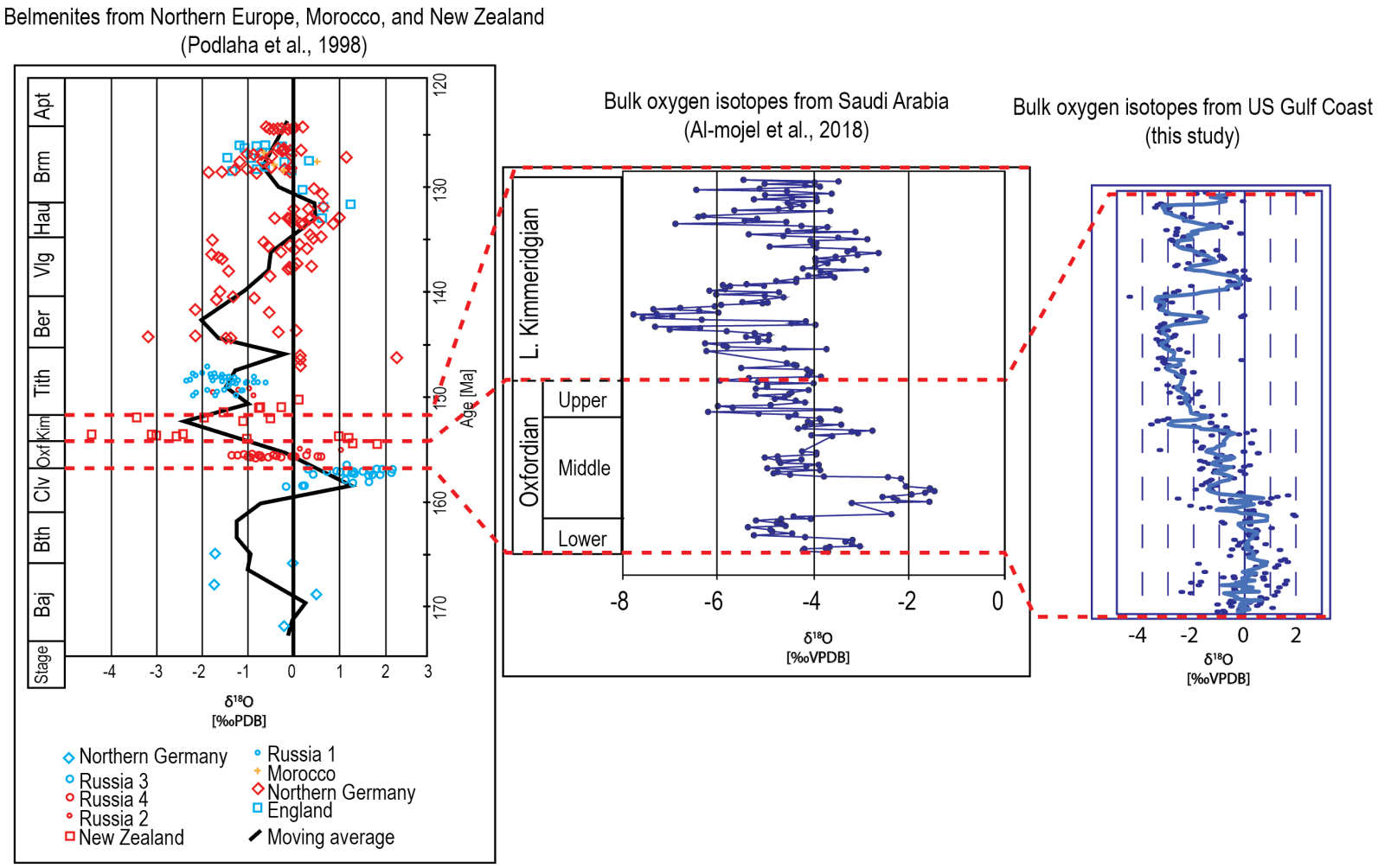
Belmenites from Northern Europe, Morocco, and New Zealand
(Podlaha et al., 1998)
Apt
Brm
Hau
Vlg
Ber
Tith
Kim
Oxf
Clv
Bth
Baj
Stage
120
130
140
150
160
170
Age [Ma]
-4
-3
-2
-1
0
1
2
3
δ18O
[‰PDB]
Northern Germany
Russia 3
Russia 4
Russia 2
New Zealand
Russia 1
Morocco
Northern Germany
England
Moving average
Bulk oxygen isotopes from Saudi Arabia
(Al-mojel et al., 2018)
L. Kimmeridgian
Oxfordian
Upper
Middle
Lower
-8
-6
-4
-2
0
δ18O
[‰VPDB]
Bulk oxygen isotopes from US Gulf Coast
(this study)
-4
-2
0
2
δ18O
[‰VPDB]

Figure 26.

Figure 26: Comparison between $\delta^{18}O_{carb}$ records of belemnite studies in northern Europe, Morocco, and New Zealand (Podlaha et al., 1998), bulk oxygen isotope studies in Saudi Arabia (Al-mojel et al., 2018), and the current study.

Pyrite

There are two main occurrences of pyrite present within the Smackover section as indicated by the XRF data, XRD data, and by petrographic observations (Fig. 8). Small (2 to 20 microns) pyrite framboids are present in the lower Smackover within organic laminae (Fig. 8E, F) and large (50 to 300 microns) pyrite framboids are present within dolomite intercrystalline pore space (Fig. 8B, C) and in large (1.5 to 2.5 cm wide and 8 to 15 cm long) open fractures (Fig. 8A, D). The pyrite types were potentially formed through bacterial sulfate reduction (BSR) and thermochemical sulfate reduction (TSR), the lower Smackover pyrite (within the laminated mudstones) being deposited early within the sediment-water-interface related to (BSR) and the large pyrite framboids (within upper Smackover dolomitized intervals) being formed during late burial due to (TSR).

The organics in the lower Smackover laminated muds are interpreted as being deposited by sulfur reducing microbial mats in an anoxic environment. Under anoxic conditions anaerobic microbes carry out metabolic processes using sulfate as the oxidant to oxidize organics (Goldstein and Aizenshtat, 1994). This sulfate reduction ultimately creates energy for the organisms and CO_2 and H_2S as byproducts (Goldstein and Aizenshtat, 1994). The free H_2S reacted with available Fe^{2+} present in the sediment likely supplied by windblown sources similar to the quartz silt or formation water. This reaction may result in the precipitation of pyrite framboids forming within the organics in the

laminated mudstones. However, they may have formed through a combination of BSR and TSR.

Deep Smackover wells commonly produce H_2S and CO_2 as uneconomic gases and create a hazard when exploring for economic quantities of hydrocarbons (Wade et al., 1989). Multiple authors have proposed these gases were formed through (TSR) at elevated thermal maturities (Sassen and Moore, 1988; Wade et al., 1989; Heydari and Moore, 1989; Sassen, 1990; Moldovanyi et al., 1990). TSR is the abiotic reaction of sulfate with organic matter to form H_2S and CO_2 (Goldstein and Aizenshtat, 1994). The TSR reaction is illustrated in the equation below showing the reaction of methane and sulfate to form carbon dioxide, hydrogen sulfide, and hydroxide ion:

$$CH_4 + SO_4^{2-} \rightarrow CO_2 + H_2S + 2OH^-$$

The specifics of what reaction pathways and which conditions are needed for this reaction to take place have been debated at length in the literature (Machel, 2001). The temperature and thermal maturities required for TSR reactions to take place vary between regions and between hydrocarbon pools within a single formation based on a variety of factors, but the range of minimum temperatures is about 100-140ºC (Machel, 2001). In Smackover strata, Sassen 1990 observed TSR reactions taking place above R_o values of 1.0-1.2%. TSR requires large amounts of available sulfate anions (SO_4^{2-}) for the reaction to take place, generally sourced by anhydrites (Machel, 2001). However, the reduction of these sulfate ions requires a significant activation energy and limits the reaction taking place (Zheng et al. 2008). Zhang et al. (2008) suggested that for the reaction to take place under reservoir conditions it requires free Mg^{2+}, forming $MgSO_4$ contact-ion-pair, as a

catalyst for the reaction. Once the reaction is initiated, its reaction rate increases with the presence of higher H_2S concentrations, leading to an exponential increase in reactivity. The Smackover system contains an abundance of Mg and sulfate sourced by the overlying Buckner anhydrite. The large secondary pyrite framboids observed within fractures and in upper Smackover dolomites were probably formed by H_2S generated through TSR reacting with Fe^{2+} present in pore fluids or ferroan dolomites. TSR can produce an acidic environment, enhancing porosity by dissolving carbonate material. Large open fractures are preserved in the core and are lined with pyrite and saddle dolomite (Fig. 8A, D). TSR may have enhanced these fractures. However, the degree of dissolution caused by TSR is debated within the literature.

Unconventional Potential

The lower Smackover is well known as a prolific source rock along the northern GOM, sourcing upper Jurassic and Cretaceous reservoirs (Wescott and Hood, 1994; Pearson, 2011). With the advent of unconventional resource exploration, prolific source rocks such as the lower Smackover are being evaluated and explored for drilling. However, there is a limited amount of core drilled through the section. Because of this, detailed core analysis of these lithofacies provide helpful insights for exploration.

The organic-rich intervals of the lower Smackover are the thin-bedded and laminated mudstones. Organic content is concentrated along carbonate poor lamina and seams. Because of this, it is unlikely to find target intervals with large volumes of organic matter and high porosity/storage potential similar to those of the Eagle Ford, Marcellas,

Bakken, among other organic-rich hydrocarbon producing formations. Instead, source rocks are spread throughout the lower Smackover section in thin seams separated by thick carbonate mudstones with low porosities as a result of dissolution and compaction. During deposition of the lower Smackover, carbonate mud sedimentation is interpreted to have inhibited the formation of bacterial mats. Because of this, identification of terrigenous-rich intervals is key to locating intervals with higher organic content.

Conventional Potential

The upper oolitic grainstones have been the main target for Smackover exploration across the Northern Gulf of Mexico. Unfortunately, in the Travis GU No. #1 core most of this interval is absent by erosion. However, dolomitized intervals in the core contain abundant intercrystalline pores with solid bitumen. These intervals have been charged with hydrocarbons and have high porosities, so they are ideal targets at favorable thermal maturities. If Smackover reservoirs are at high temperatures and maturities, there is a risk of thermochemical sulfate reduction. This process converts hydrocarbons to uneconomic gases causing potential drilling complications and reduced profitability. The overlying Buckner Anhydrite may have supplied the sulfate needed for thermochemical sulfate reactions to occur leading to increasing H_2S generation. If this is the case, then there is an associated risk with exploring for reservoirs sealed by the Buckner. While the unit is an effective seal it may also lead to increased destruction of economic gas through TSR. This should be taken into consideration for future exploration.

CHAPTER 6: CONCLUSION

The Travis GU No. 1 core contains the majority of Smackover section and provides a continuous record of its deposition and associated lithofacies. Additionally, XRD and XRF data characterizes primary and secondary mineralogy along the length of the core. This makes it an ideal type-cored section for the East Texas basin and will be valuable for future regional and global studies.

Lower Smackover mudstones are interpreted as being deposited by sulfur reducing bacterial mats (thin intervals) and gravity flows in a distal ramp environment. TOC data and lithofacies trends suggest organic matter accumulation is inhibited by carbonate sedimentation. Organic matter is concentrated along laminae and seams preventing the development of large volumes of rock with high TOC and porosity. This limits the lower Smackover's prospectivity as an unconventional resource. However, these features may have contributed to the lower Smackover's ability to generate and expel hydrocarbons efficiently.

The Smackover section represents a progression of shallowing lithofacies characteristic of a prograding ramp. The proposed depositional model shows lithofacies and ramp locations defined by the position of the anoxic bottom-water layer and energy related to fair-weather and storm-wave base. Changes between thin-bedded and bioturbated muds and frequency of gravity flow deposits may reflect fourth-order cycles. The grainstones that formed in oolitic shoals, characteristic of the upper Smackover, are

truncated by an unconformable contact with the overlying Buckner Anhydrite. Previous studies have concluded that during Buckner deposition dense Mg-rich brines filtered through the Smackover strata below and replaced porous lithofacies with dolomite through reflux dolomitization (Budd and Loucks, 1981; Harwood and Fontana, 1983; Hancharik, 1984; Stewart, 1984; Koepnick et al., 1985; Moore et al., 1988). This process enhanced the porosity of multiple intervals and formed potential reservoir.

The XRF data shows multiple trends along the length of the core. In the lower Smackover, there are cycles of increasing Si concentrations which are probably produced by variations in sediment supply. These high Si intervals commonly contain higher TOC's. Correlation between Fe and S curves represent the presence of pyrite. This pyrite is detected in XRF and observed in thin section within organic-rich intervals of the lower Smackover as well as in solid bitumen in upper Smackover reservoir rock. Intervals with high Sr are present within the core and correspond to celestine minerals formed during early burial diagenesis from Sr-rich diagenetic fluids. These Sr-rich fluids were possibly sourced from the release of Sr by Sr-bearing aragonites converting to calcite during early burial.

The isotope data from the investigated core forms the first secular curve taken through the Smackover Formation. The inorganic and organic carbon isotope data contain excursions that correlate to global curves. When compared to global curves, the inorganic carbon data is bulk shifted towards heavier values by 1.5‰. This may suggest some local effects that sequester light carbon or restrict access to light carbon sources. Oxygen

isotopic data has high amounts of variability and is affected by dolomitization but does show a 3‰ excursion towards light isotopic values that is consistent with global trends.

References

Ahr, W. M., 1973, The carbonate ramp; an alternative to the shelf model: Transactions - Gulf Coast Association of Geological Societies, v. 23, p. 221-225.

Al-Mojel, A., G. Dera, P. Razin, and Y.-M. Le Nindre, 2018, Carbon and oxygen isotope stratigraphy of Jurassic platform carbonates from Saudi Arabia; implications for diagenesis, correlations and global paleoenvironmental changes: Palaeogeography, Palaeoclimatology, Palaeoecology, v. 511, p. 388-402.

Allan, J., and R. Matthews, 1982, Isotope signatures associated with early meteoric diagenesis: Sedimentology, v. 29, p. 797-817.

Bebout, D. G., and R. G. Loucks, 1984, Handbook for logging carbonate rocks, Bureau of Economic Geology, University of Texas at Austin.

Budd, D. A., and R. G. Loucks, 1981, Smackover and Lower Buckner Formations, South Texas: depositional systems on a Jurassic carbonate ramp, Bureau of Economic Geology, University of Texas at Austin.

Burchette, T. P., and V. P. Wright, 1992, Carbonate ramp depositional systems: Sedimentary Geology, v. 79, p. 3-57.

Claypool, G. E., and E. A. Mancini, 1989, Geochemical relationships of petroleum in Mesozoic reservoirs to carbonate source rocks of Jurassic Smackover Formation, southwestern Alabama: AAPG Bulletin, v. 73, p. 904-924.

Dickinson, K. A., 1968, Upper Jurassic stratigraphy of some adjacent parts of Texas, Louisiana, and Arkansas.

Dickinson, K. A., 1969, Upper Jurassic Carbonate Rocks in Northeastern Texas and Adjoining Parts of Arkansas and Louisiana (1).

Dunham, R. J., 1962, Classification of carbonate rocks according to depositional texture: Memoir - American Association of Petroleum Geologists, p. 108-121.

Edwards, C. T., M. R. Saltzman, S. A. Leslie, S. M. Bergstrom, A. R. C. Sedlacek, A. Howard, J. A. Bauer, W. C. Sweet, and S. A. Young, 2015, Strontium isotope ((super 87) Sr/ (super 86) Sr) stratigraphy of Ordovician bulk carbonate; implications for preservation of primary seawater values: Geological Society of America Bulletin, v. 127, p. 1275-1289.

Eltom, H. A., L. A. Gonzalez, S. T. Hasiotis, E. C. Rankey, and D. L. Cantrell, 2018, Paleogeographic and paleo-oceanographic influences on carbon isotope signatures; implications for global and regional correlation, Middle-Upper Jurassic of Saudi Arabia: Sedimentary Geology, v. 364, p. 89-102.

Ewing, T. E., 2001, Review of Late Jurassic depositional systems and potential hydrocarbon plays of the northern Gulf of Mexico Basin: AAPG Bulletin, v. 85, p. 1699.

Ewing, T. E., 2009, The ups and downs of the Sabine uplift and the northern Gulf of Mexico Basin: Jurassic basement blocks, Cretaceous thermal uplifts, and Cenozoic flexure.

Flugel, E., 2004, Microfacies of carbonate rocks; analysis, interpretation and application, Springer, Berlin, Federal Republic of Germany, 976 p.

Föllmi, K. B., A. Godet, S. Bodin, and P. Linder, 2006, Interactions between environmental change and shallow water carbonate buildup along the northern Tethyan margin and their impact on the Early Cretaceous carbon isotope record: Paleoceanography, v. 21.

Goldhammer, R. K., 1998, Second-order accommodation cycles and points of stratigraphic turnaround; implications for high-resolution sequence stratigraphy and facies architecture of the Haynesville and Cotton Valley Lime pinnacle reefs of the East Texas salt basin: The Bulletin of the Houston Geological Society, v. 40, p. 16-19.

Goldstein, T., and Z. Aizenshtat, 1994, Thermochemical sulfate reduction a review: Journal of Thermal Analysis and Calorimetry, v. 42, p. 241-290.

Hancharik, J. M., 1984, Facies analysis and petroleum potential of the Jurassic Smackover Formation, western and northern areas, East Texas Basin.

Harwood, G., and C. M. Fontana, 1983, Smackover deposition and diagenesis and structural history of the Bryan's Mill area, Cass and Bowie Counties, Texas, Department of Geology, Louisiana State University and Agricultural and ….

Heydari, E., and L. Baria, 2005a, A conceptual model for the sequence stratigraphy of the Smackover Formation in north-central U.S. Gulf Coast: Transactions - Gulf Coast Association of Geological Societies, v. 55, p. 321-340.

Heydari, E., and L. Baria, 2005b, A conceptual model for the sequence stratigraphy of the Smackover Formation in north-central US Gulf Coast.

Heydari, E., and C. H. Moore, 1989, Burial diagenesis and thermochemical sulfate reduction, Smackover Formation, southeastern Mississippi salt basin: Geology (Boulder), v. 17, p. 1080-1084.

Heydari, E., and C. H. Moore, 1994, Paleoceanographic and paleoclimatic controls on ooid mineralogy of the Smackover Formation, Mississippi salt basin; implications for Late Jurassic seawater composition: Journal of Sedimentary Research, Section A: Sedimentary Petrology and Processes, v. 64, p. 101-114.

Heydari, E., W. J. Wade, and L. C. Anderson, 1997, Depositional environments, organic carbon accumulation, and solar-forcing cyclicity in Smackover Formation lime mudstones, northern Gulf Coast: AAPG Bulletin, v. 81, p. 760-774.

Immenhauser, A., G. Della Porta, J. A. M. Kenter, and J. R. Bahamonde, 2003, An alternative model for positive shifts in shallow-marine carbonate delta (super 13) C and delta (super 18) O: Sedimentology, v. 50, p. 953-959.

Jackson, M., 1982, Fault tectonics of the East Texas Basin: Geological Circular - Texas, University, Bureau of Economic Geology, University of Texas at Austin, Bureau of Economic Geology, Austin, TX, United States, 31 p.

Jackson, M., and S. Seni, 1983, Geometry and evolution of salt structures in a marginal rift basin of the Gulf of Mexico, east Texas: Geology, v. 11, p. 131-135.

Jenkyns, H. C., C. E. Jones, D. R. Groecke, S. P. Hesselbo, and D. N. Parkinson, 2002, Chemostratigraphy of the Jurassic system; applications, limitations and implications for palaeoceanography: Journal of the Geological Society of London, v. 159, Part 4, p. 351-378.

Kinsman, D. J. J., 1969, Interpretation of Sr (super +2) concentrations in carbonate minerals and rocks: Journal of Sedimentary Petrology, v. 39, p. 486-508.

Koepnick, R. B., D. E. Eby, and K. C. King, 1985, Controls on porosity and dolomite distribution in upper Smackover Formation (Upper Jurassic), southwestern Alabama and western Florida: AAPG Bulletin, v. 69, p. 274.

Land, L. S., 1980, The isotopic and trace element geochemistry of dolomite; the state of the art: Special Publication - Society of Economic Paleontologists and Mineralogists, p. 87-110.

Law, C. A., 1999, Evaluating source rocks: AAPG Special Volumes. Treatise of Petroleum Geology/Handbook of Petroleum Geology, v. 3, p. 6-1.

Locklin, A. C., 1984, Curry Field (Smackover), East Texas Basin; with a brief history of the exploration of the Mexia-Talco fault system: The Jurassic of East Texas, p. 32-42.

Loucks, R., and M. Longman, 1987, Lower Cretaceous Ferry Lake Anhydrite, Fairway field, east Texas: product of shallow-subtidal deposition.

Louis-Schmid, B., P. Rais, S. M. Bernasconi, P. Pellenard, P.-Y. Collin, and H. Weissert, 2007, Detailed record of the mid-Oxfordian (Late Jurassic) positive carbon-isotope excursion in two hemipelagic sections (France and Switzerland); a plate tectonic trigger?: Palaeogeography, Palaeoclimatology, Palaeoecology, v. 248, p. 459-472.

Machel, H. G., 2001, Bacterial and thermochemical sulfate reduction in diagenetic settings; old and new insights: Sedimentary Geology, v. 140, p. 143-175.

Malek-Aslani, M., 1973, Environmental Modeling: A Useful Exploration Tool in Carbonates.

Mancini, E. A., J. C. Llinas, W. C. Parcell, M. Aurell, B. Badenas, R. R. Leinfelder, and D. J. Benson, 2004, Upper Jurassic thrombolite reservoir play, northeastern Gulf of Mexico: AAPG Bulletin, v. 88, p. 1573-1602.

Mancini, E. A., W. C. Parcell, and T. M. Puckett, 2003, Oxfordian carbonate petroleum system characterization and modeling; Upper Jurassic Smackover Formation, northeastern Gulf of Mexico, USA: American Association of Petroleum Geologists International Conference Abstracts, v. 2003.

Mann, S. D., 1988, Subaqueous evaporites of the Buckner Member, Haynesville Formation, northeastern Mobile County, Alabama: Transactions - Gulf Coast Association of Geological Societies, v. 38, p. 187-196.

Mann, S. D., and D. C. Kopaska-Merkel, 1992, Depositional history of the Smackover-Buckner transition, eastern Mississippi interior salt basin: Transactions - Gulf Coast Association of Geological Societies, v. 42, p. 245-265.

Martin, R. G., 1978, Northern and Eastern Gulf of Mexico Continental Margin: Stratigraphic and Structural Framework: 1. The Setting.

Matyszkiewicz, J., 1993, Genesis of stromatactis in an Upper Jurassic carbonate buildup (Mlynka, Cracow region, southern Poland); internal reworking and erosion of organic growth cavities: Facies, v. 28, p. 87-96.

Mitchell-Tapping, H. J., 1984, Depositional environment of the updip Smackover area of East Texas: The Jurassic of East Texas, p. 79-86.

Moldovanyi, E. P., L. M. Walter, J. C. Brannon, and F. A. Podosek, 1990, New constraints on carbonate diagenesis from integrated Sr and S isotopic and rare

earth element data, Jurassic Smackover Formation, U.S. Gulf Coast: Applied Geochemistry, v. 5, p. 449-470.

Moore, C. H., 1997, Sequence stratigraphic framework of Upper Jurassic Oxfordian Smackover equivalents illustrated by the Humble McKean #12 core, Buckner Field, southern Arkansas, central Gulf of Mexico, USA: CSPG-SEPM joint convention; Sedimentary events, hydrocarbon systems, p. 305-315.

Moore, C. H., A. Chowdhury, and L. Chan, 1988, Upper Jurassic Smackover platform dolomitization, northwestern Gulf of Mexico; a tale of two waters: Technical Series Contribution - Applied Carbonate Research Program, v. 50.

Nunn, E. V., and G. D. Price, 2010, Late Jurassic (Kimmeridgian–Tithonian) stable isotopes (δ18O, δ13C) and Mg/Ca ratios: new palaeoclimate data from Helmsdale, northeast Scotland: Palaeogeography, Palaeoclimatology, Palaeoecology, v. 292, p. 325-335.

O'Dogherty, L., R. Aguado, P. O. Baumgartner, M. Bill, S. Gorican, J. Sandoval, and L. Sequeiros, 2018, Carbon-isotope stratigraphy and pelagic biofacies of the Middle-Upper Jurassic transition in the Tethys-Central Atlantic connection: Palaeogeography, Palaeoclimatology, Palaeoecology, v. 507, p. 129-144.

Oschmann, W., 1993, Environmental oxygen fluctuations and the adaptive response of marine benthic organisms: Journal of the Geological Society of London, v. 150, p. 187-191.

Pearson, O. N., 2011, Undiscovered hydrocarbon resources in the US Gulf Coast Jurassic Norphlet and Smackover formations: Transactions - Gulf Coast Association of Geological Societies, v. 61, p. 329-340.

Pilger, R. H., Jr., 1981, The opening of the Gulf of Mexico; implications for the tectionic evolution of the northern Gulf Coast: Transactions - Gulf Coast Association of Geological Societies, v. 31, p. 377-381.

Pindell, J., and L. Kennan, 2001, Kinematic evolution of the Gulf of Mexico and Caribbean: Program and Abstracts - Society of Economic Paleontologists. Gulf Coast Section. Research Conference, v. 21, p. 193-220.

Podlaha, O. G., J. Mutterlose, and J. Veizer, 1998, Preservation of delta (super 18) O and delta (super 13) C in belemnite rostra from the Jurassic/Early Cretaceous successions: American Journal of Science, v. 298, p. 324-347.

Pratt, B. R., 2001, Calcification of cyanobacterial filaments; girvanella and the origin of lower Paleozoic lime mud: Geology (Boulder), v. 29, p. 763-766.

Saltzman, M. R., and E. Thomas, 2012, Carbon isotope stratigraphy in the geologic time scale 2012: Abstracts with Programs - Geological Society of America, v. 44, p. 589.

Salvador, A., 1987, Late Triassic-Jurassic paleogeography and origin of Gulf of Mexico basin: AAPG Bulletin, v. 71, p. 419-451.

Sandberg, P. A., 1983, An oscillating trend in Phanerozoic non-skeletal carbonate mineralogy: Nature, v. 305, p. 19.

Sassen, R., 1990, Geochemistry of carbonate source rocks and crude oils in Jurassic salt basins of the Gulf Coast: Proceedings of the Annual Research Conference, Gulf Coast Section, Society of Economic Paleontologists and Mineralogists Foundation, v. 9, p. 11-22.

Sassen, R., and C. H. Moore, 1988, Framework of hydrocarbon generation and destruction in eastern Smackover trend: AAPG Bulletin, v. 72, p. 649-663.

Sassen, R., C. H. Moore, and F. C. Meendsen, 1987, Distribution of hydrocarbon source potential in the Jurassic Smackover Formation: Organic Geochemistry, v. 11, p. 379-383.

Schieber, J., P. K. Bose, P. G. Eriksson, S. Banerjee, S. Sarkar, W. Altermann, and O. Catuneanu, 2007, Atlas of microbial mat features preserved within the siliciclastic rock record, v. 2.

Schreiber, B. C., R. Catalano, and E. Schreiber, 1977, An evaporitic lithofacies continuum; latest Miocene (Messinian) deposits of Salemi Basin (Sicily) and a modern analog: Studies in Geology (Tulsa), p. 169-180.

Schreiber, B. C., M. S. Roth, and M. L. Helman, 1982, Recognition of primary facies characteristics of evaporites and the differentiation of these forms from diagenetic overprints: SEPM Core Workshop, v. 3, p. 1-32.

Seni, S., and M. Jackson, 1983, Evolution of salt structures, east Texas diapir province, part 1: Sedimentary record of halokinesis: AAPG Bulletin, v. 67, p. 1219-1244.

Shackleton, N. J., 1987, Oxygen isotopes, ice volume and sea level: Quaternary Science Reviews, v. 6, p. 183-190.

Shinn, E. A., 1983, Tidal flat environment: AAPG Memoir, v. 33, p. 171-210.

Stewart, S. K., 1984, Smackover and Haynesville facies relationships in north-central East Texas: The Jurassic of East Texas, p. 56-62.

Thompson, J. B., and F. G. Ferris, 1990, Cyanobacterial precipitation of gypsum, calcite, and magnesite from natural alkaline lake water: Geology (Boulder), v. 18, p. 995-998.

Turner, J. R., 2001, Evidence for strike-slip faulting in the Smackover Formation of Northeast Texas and South Arkansas and its geological implications: Transactions - Gulf Coast Association of Geological Societies, v. 51, p. 339-347.

Wade, W. J., J. S. Hanor, and R. Sassen, 1989, Controls on H (sub 2) S concentration and hydrocarbon destruction in the eastern Smackover Trend: Transactions - Gulf Coast Association of Geological Societies, v. 39, p. 309-320.

Wade, W. J., and C. H. Moore, 1993, Jurassic sequence stratigraphy of southwest Alabama.

Wanless, H. R., L. P. Tedesco, and K. M. Tyrrell, 1988, Production of subtidal tubular and surficial tempestites by Hurricane Kate, Caicos Platform, British West Indies: Journal of Sedimentary Petrology, v. 58, p. 739-750.

Warren, J. K., 2006, Evaporites; sediments, resources, and hydrocarbons, Springer Berlin Heidelberg, New York, NY, United States, 1035 p.

Weissert, H., and E. Erba, 2004, Volcanism, CO (sub 2) and palaeoclimate; a Late Jurassic-Early Cretaceous carbon and oxygen isotope record: Journal of the Geological Society of London, v. 161, p. 695-702.

Wescott, W. A., and W. C. Hood, 1994, Hydrocarbon generation and migration routes in the East Texas Basin: AAPG Bulletin, v. 78, p. 287-307.

Wierzbowski, A., A. L. Coe, M. W. Hounslow, B. A. MATYJA, J. G. Ogg, K. N. Page, H. Wierzbowski, and J. K. Wright, 2006, A potential stratotype for the Oxfordian/Kimmeridgian boundary: Staffin Bay, Isle of Skye, UK: Volumina Jurassica, v. 4, p. 17-33.

Wierzbowski, H., 2015, Seawater temperatures and carbon isotope variations in central European basins at the Middle–Late Jurassic transition (Late Callovian–Early Kimmeridgian): Palaeogeography, Palaeoclimatology, Palaeoecology, v. 440, p. 506-523.

Wierzbowski, H., K. Dembicz, and T. Praszkier, 2009, Oxygen and carbon isotope composition of Callovian–Lower Oxfordian (Middle–Upper Jurassic) belemnite

rostra from central Poland: A record of a Late Callovian global sea-level rise?: Palaeogeography, Palaeoclimatology, Palaeoecology, v. 283, p. 182-194.

Wierzbowski, H., M. A. Rogov, B. A. Matyja, D. Kiselev, and A. Ippolitov, 2013, Middle–Upper Jurassic (Upper Callovian–Lower Kimmeridgian) stable isotope and elemental records of the Russian Platform: Indices of oceanographic and climatic changes: Global and Planetary Change, v. 107, p. 196-212.

Wilkinson, S., 1984, Upper Jurassic facies relationships and their interdependence on salt tectonism in Rains, Van Zandt, and adjacent counties, East Texas: The Jurassic of East Texas, p. 153-156.

Wood, M. L., and J. L. Walper, 1974, The Evolution of the Interior Mesozoic Basin and the Gulf of Mexico.

Zhang, T., A. Amrani, G. S. Ellis, Q. Ma, and Y. Tang, 2008, Experimental investigation on thermochemical sulfate reduction by H2S initiation: Geochimica et Cosmochimica Acta, v. 72, p. 3518-3530.